RESEARCH ARTICLE

Endothelial cell signature in muscle stem cells validated by VEGFA-FLT1-AKT1 axis promoting survival of muscle stem cell

Mayank Verma[1,2,3,4], Yoko Asakura[2,3,4], Xuerui Wang[2,3,4], Kasey Zhou[2,3,4], Mahmut Ünverdi[2,3,4], Allison P Kann[5,6], Robert S Krauss[5,6], Atsushi Asakura[2,3,4]*

[1]Department of Pediatrics & Neurology, Division of Pediatric Neurology, The University of Texas Southwestern Medical Center, Dallas, United States; [2]Stem Cell Institute, University of Minnesota Medical School, Minneapolis, United States; [3]Greg Marzolf Jr. Muscular Dystrophy Center, University of Minnesota Medical School, Minneapolis, United States; [4]Department of Neurology, University of Minnesota Medical School, Minneapolis, United States; [5]Department of Cell, Developmental, and Regenerative Biology, Icahn School of Medicine at Mount Sinai, New York, United States; [6]Graduate School of Biomedical Sciencesf, Icahn School of Medicine at Mount Sinai, New York, United States

Abstract Endothelial and skeletal muscle lineages arise from common embryonic progenitors. Despite their shared developmental origin, adult endothelial cells (ECs) and muscle stem cells (MuSCs; satellite cells) have been thought to possess distinct gene signatures and signaling pathways. Here, we shift this paradigm by uncovering how adult MuSC behavior is affected by the expression of a subset of EC transcripts. We used several computational analyses including single-cell RNA-seq (scRNA-seq) to show that MuSCs express low levels of canonical EC markers in mice. We demonstrate that MuSC survival is regulated by one such prototypic endothelial signaling pathway (VEGFA-FLT1). Using pharmacological and genetic gain- and loss-of-function studies, we identify the FLT1-AKT1 axis as the key effector underlying VEGFA-mediated regulation of MuSC survival. All together, our data support that the VEGFA-FLT1-AKT1 pathway promotes MuSC survival during muscle regeneration, and highlights how the minor expression of select transcripts is sufficient for affecting cell behavior.

***For correspondence:** asakura@umn.edu

Competing interest: The authors declare that no competing interests exist.

Funding: See page 18

Preprinted: 28 August 2021
Received: 02 September 2021
Accepted: 05 June 2024
Published: 06 June 2024

Reviewing Editor: Tom H Cheung, The Hong Kong University of Science and Technology, Hong Kong

Editor's evaluation

This study presents a valuable finding on the unique role of VEGFA-FLT1-AKT1 signaling in regulating muscle stem cell (MuSC) survival. The evidence supporting the claims is convincing, with multiple approaches utilized, including pharmacological and genetic methods performed in vitro and in vivo, demonstrating that the VEGFA-FLT1-AKT1 axis protected MuSCs from apoptosis. The work will be of broad interest to researchers in the MuSC biology field and support the future development of VEGFA and FLT1 targeted therapies for various diseases, such as cancer and neuromuscular diseases.

Introduction

Skeletal muscle and endothelial cells (ECs) and their progenitors from the trunk and limbs are derived from the somites during early developments. Previous works demonstrated the existence of bipotent progenitors which express both *Pax3* and *Flk1* (***Eichmann et al., 1993***; ***Kardon et al., 2002***;

Ema et al., 2006; ***Esner et al., 2006***; ***Tozer et al., 2007***). These bipotent progenitors migrate into trunk and limb buds from ventrolateral region of the somites to generate MYOD(+) myogenic cells followed by skeletal muscle and PECAM1(+) ECs followed by vasculatures (***Hutcheson and Kardon, 2009***; ***Kardon et al., 2002***; ***Lagha et al., 2009***; ***Mayeuf-Louchart et al., 2016***; ***Mayeuf-Louchart et al., 2014***). In addition, FLK1(+) cells give rise to myogenic cells during development and oncologic transformation (***Drummond and Hatley, 2018***; ***Mayeuf-Louchart et al., 2014***; ***Motoike et al., 2003***). Lastly, multipotent mesoangioblasts, vessel-associated stem cells, have been identified in embryonic dorsal aorta (***Minasi et al., 2002***). These cells are able to differentiate into several types of mesodermal tissues including skeletal muscle and ECs (***Roobrouck et al., 2011***). Interestingly, these myogenic cells show the same morphology as muscle satellite cells (MuSCs), stem cell populations for skeletal muscle, and express a number of myogenic and EC markers such as *Myod*, *Cdh15*, *Kdr,* and *Cdh5* (***De Angelis et al., 1999***). However, it is not clear whether adult MuSCs derived from these bipotent progenitors still maintain canonical EC signals. Curiously, blood vessel-associated myoendothelial cell progenitors that express both myogenic and EC markers, and are able to differentiate into myogenic cells following transplantation have been identified in the interstitial spaces of both murine and human adult skeletal muscle (***Tamaki et al., 2002***; ***Zheng et al., 2007***; ***Huang et al., 2014***). However, the relationship between these myoendothelial cell progenitors and MuSCs remains unclear.

Vascular endothelial growth factor (VEGF), specifically VEGFA modulates many biological aspects including angiogenesis through its two receptors, FLT1 and FLK1. Although FLK1 possesses stronger signaling capability and the major signaling receptor tyrosine kinase (RTK) for VEGFA, FLT1 has considerably higher affinity for VEGF but weaker cytoplasmic signaling capability. In normal tissue, FLT1 acts as a decoy receptor and a sink trap for VEGF thereby preventing excessive normal and pathological angiogenesis. In addition, there are two co-receptors for VEGFA (NRP1 and NRP2) that function with FLK1 to modulate VEGFA signaling. While VEGF signaling has been extensively studied for its role in development, proliferation, and survival of endothelial cells (ECs), its role in non-vascular systems such as neuron and bone has only recently been appreciated (***Poesen et al., 2008***; ***Liu et al., 2012***; ***Okabe et al., 2014***). Skeletal muscle tissue is the most abundant producer of VEGFA in the body. It has already been extensively studied in the skeletal muscle fibers in models of *Vegfa* knockout mice (***Tang et al., 2004***; ***Wagner et al., 2006***; ***Olfert et al., 2009***) as well as *Vegfa* overexpression (***Arsic et al., 2004***; ***Yan et al., 2005***; ***Messina et al., 2007***; ***Bouchentouf et al., 2008***).

Adult skeletal muscle also contains the tissue resident muscle stem cell population, termed MuSCs, which mediate postnatal muscle growth and muscle regeneration (***Motohashi and Asakura, 2014***). After muscle injury, quiescent MuSCs initiate proliferation to produce myogenic precursor cells, or myoblasts. The myoblasts undergo multiple rounds of cell division before terminal differentiation and formation of multinucleated myotubes by cell fusion. Importantly, the MuSC-derived myoblasts also express VEGFA, which has been shown to increase the proliferation of myoblasts (***Christov et al., 2007***). Our data obtained from genetical model mice demonstrated that MuSCs express abundant VEGFA, which recruits ECs to establish vascular niche for MuSC self-renewal and maintenance (***Verma et al., 2018***). In addition, VEGFA and its receptors are expressed in the myoblast cell line, C2C12 cells, and the signaling can induce cell migration and protect apoptotic cell during myogenic differentiation in vitro (***Germani et al., 2003***; ***Bryan et al., 2008***; ***Mercatelli et al., 2010***). However, it is not clear whether MuSCs also express VEGF receptors and if cell-autonomous VEGFA signaling plays an essential roles in MuSC function during muscle regeneration in vivo.

We have previously shown that *Flt1* heterozygous gene knockout and conditional deletion of *Flt1* in ECs display increased capillary density in skeletal muscle, indicating the essential roles for *Flt1* in adult skeletal muscle. More importantly, when crossed with the Duchenne muscular dystrophy (DMD) model *mdx* mice, these mice show both histological and functional improvements of their dystrophic phenotypes. This was partly due to the effect of increased ECs leading to an increase in MuSCs (***Verma et al., 2010***; ***Verma et al., 2019***; ***Bosco et al., 2021***). However, the effect of VEGFA on MuSC in vivo remained unknown. We found that MuSCs express low levels of canonical EC markers including VEGF receptors using single cell transcriptomics. Therefore, we examined the effects of VEGFA on MuSCs and show that it has a drastic effect on cell survival in the via its receptor FLT1 by signaling through AKT1.

Results

EC gene signal including *Vegf receptors* in MuSCs

EC signatures in MuSCs has been seen in several gene expression data sets (***Figure 1—figure supplement 1A–1D***, ***Supplementary file 1***; ***Fukada et al., 2007***; ***Charville et al., 2015***; ***Ryall et al., 2015***; ***van Velthoven et al., 2017***). However, with the lack of EC control, we questioned whether these were true expression or artifact. To isolate EC and MuSC populations, we first crossed the *Flk1*$^{+/GFP}$ mice to label the ECs of the vasculature (***Ema et al., 2006***) and the *Pax7*$^{+/CreERT2}$*:ROSA26*$^{+/Loxp\text{-}stop\text{-}Loxp\text{-}tdTomato}$ (*Pax7*$^{+/CreERT2}$*:R26R*$^{+/tdT}$) mice to mark the MuSC lineage (***Murphy et al., 2011***; ***Verma et al., 2018***). We performed bulk RNA sequencing (RNA-seq) on FACS sorted ECs and MuSCs as well as freshly isolated single muscle fibers (***Figure 1A***, ***Figure 1—figure supplement 1E–G***). We found that single muscle fibers routinely have ECs fragments attached to the fiber (***Figure 1—figure supplement 1G***) and so we removed such fibers based on *Flk1*^{GFP} expression from the samples collected for sequencing. We surveyed for canonical genes for each cell type (***Figure 1B***) and found minimal but reliable expression of canonical ECs genes such as *Pecam1*, *Cdh5*, *Kdr*, and *Flt1* in MuSCs.

It is possible that these EC signatures detected in MuSCs were due to small amounts of contaminating ECs with very high expression of the canonical EC genes skewing the average expression in MuSC RNA samples. To rule out this possibility, we performed single-cell RNA-seq (scRNA-seq) on MuSCs and ECs isolated from mouse hind limb muscle from both basal condition and 3 days post intramuscular cardiotoxin (CTX) injury to look at both quiescent and activated MuSCs from the reporter mice specified above (***Figure 1A***). We could reliably delineate injured and activated MuSCs via side and forward scatter (***Figure 1—figure supplement 1H and I***). We FACS isolated cells from both days separately and spiked in 20% of the ECs into the MuSCs from their respective time points, and performed scRNA-seq for each time point (***Figure 1A***). We performed sequencing with ~300 K read/cell compared with the commonly used sequencing with 60 K reads/cell, in order to maximize the possibility of detecting low-abundance transcripts (***Zhang et al., 2020***). In the aggregated dataset, the MuSCs showed low overlap between D0 and D3 owing to the different stages of the myogenic differentiation cycle, while the ECs clusters showed near perfect overlap (***Figure 1C and D***). While drastic morphological changes in ECs have been shown during muscle regeneration (***Hardy et al., 2016***), transcriptomic changes are much more tapered, especially compared with MuSCs (***Latroche et al., 2017***). We were able to deconvolve the quiescent MuSCs from the activated and differentiating MuSCs, ECs, and other cell types from gene signatures. (***Figure 1—figure supplement 1J***). Importantly, data from scRNA-seq were able to recapitulate the minimal expression of canonical EC genes in the MuSC clusters such as *Cdh5* (***Figure 1E***) as seen in our Bulk RNA-seq results (***Figure 1B***). These included the Vegf receptors *Flk1* (*Kdr*) and *Flt1* (***Figure 1E***).

As a quality control measure, we introduced an artificial chromosome into our reference genome with sequences for the three transgene genes; *eGFP* from *Flk1*$^{+/GFP}$, *tdTomato* and *CreERT2* from *Pax7*$^{+/CreERT2}$*:R26R*$^{+/tdT}$ and used this genome to map our single cell RNA-seq data (***Figure 1E***, ***Figure 1—figure supplement 1K***). Surprisingly, we also found *eGFP* in the MuSCs and *tdTomato* in EC fraction, while the *CreERT2* expression remained mainly restricted to the MuSCs (***Figure 1—figure supplement 1K***). FACS analysis and FACS-sorted cells confirmed that GFP(+) and tdTomato(+) cells are exclusively restricted as ECs and MuSCs, respectively (***Figure 1—figure supplement 1E and F***). Therefore, we hypothesized that this was due to the ambient-free mRNA from the digested cells that is intrinsic to any droplet based single-cell sequencing platform. By using SoupX (***Young and Behjati, 2020***), we performed careful background subtraction using genes expressed exclusively in myofibers as our negative control and genes validated by in situ hybridization as a positive control (***Kann and Krauss, 2019***). We observed decreased but sustained *eGFP* expression in the MuSC fraction and *tdTomato* expression in the EC fraction after SoupX subtraction (***Figure 1—figure supplement 1K***). In addition, the EC signatures such as *Cdh5* expression in the MuSC fraction was also sustained. These results conclude that MuSCs contain mRNAs from canonical ECs genes. We showed that the canonical EC genes, such as *Cdh5*, *Flt1* and *Flk1* were broadly expressed in the myogenic cells in our dataset (***Figure 1E***).

Since detection of rare subpopulation in single cell dataset is a factor of cell numbers, we re-analyzed previously published dataset with 2,232 myogenic cells across different states (***Torre et al., 2018***; ***De Micheli et al., 2020***). We were able to classify cell as quiescent, proliferative vs. differentiating states based on the expression of *Calcr*, *Cdk1*, and *Myog*, respectively (***Figure 1—figure***

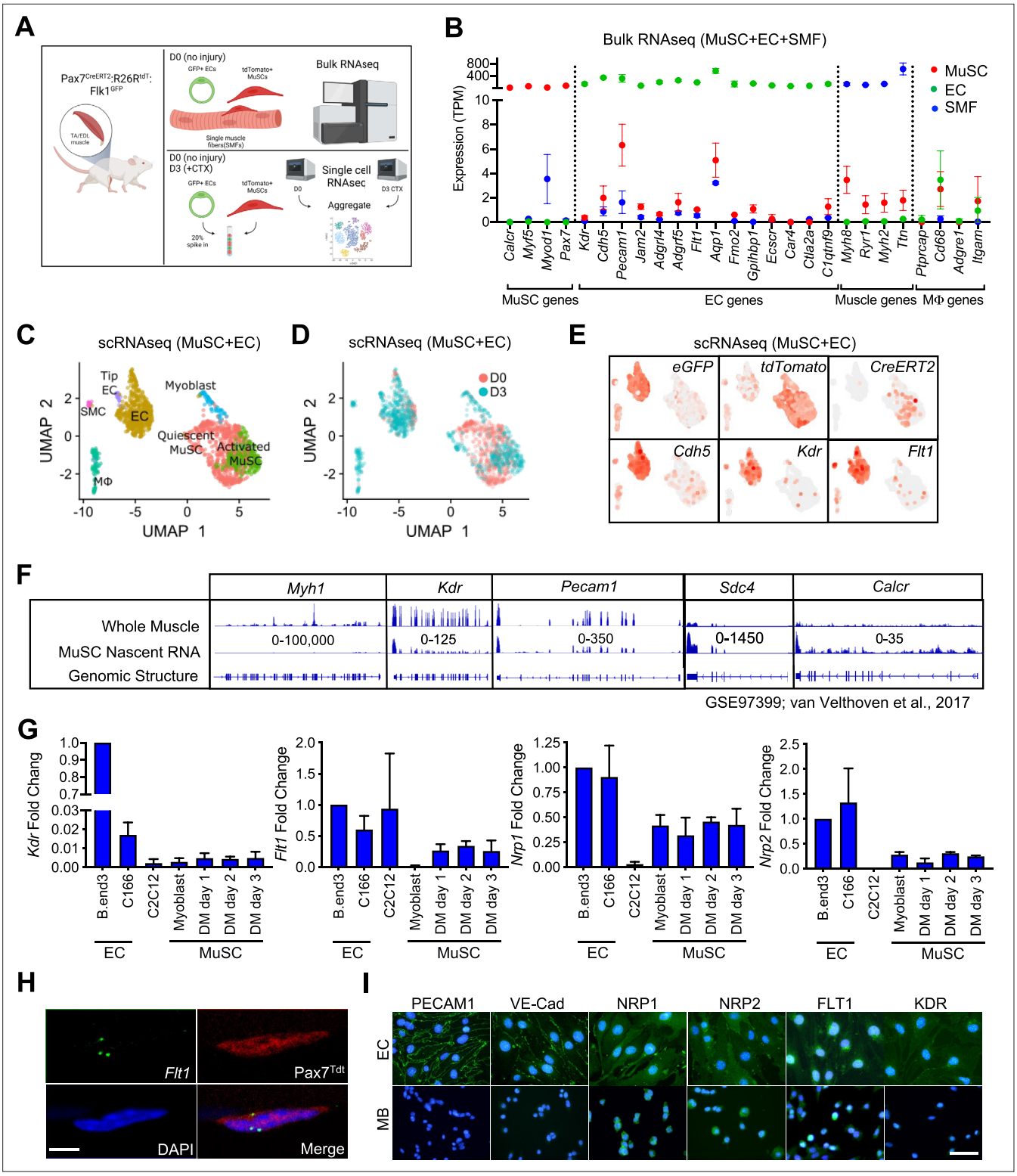

Figure 1. EC gene signal including VEGF receptor genes in MuSCs. (**A**) Experimental schema for bulk and scRNA-seq from the *Pax7*^{CreERT2}:*R26R*^{tdT}:*Flk1*^{GFP} mice. Bulk RNA-seq performed on MuSCs, ECs and single muscle fibers (SMFs) from uninjured muscle. FACS sorted MuSCs and ECs from uninjured and regenerating TA muscle (3 days following CTX) were run separately on the 10 X single cell platform and aggregated. This panel created with BioRender.com, and published using a BW26O8AXHL license with permission. (**B**) Bulk RNA-seq showing EC signature in MuSCs. Subset dividing genes that are commonly used to delineate cell identity for MuSCs, ECs and SMFs. Last column shows genes that define macrophages (Mφ), which should not be highly expressed in any on our cell types. Red dots indicate MuSCs, green dots indicate ECs and blue dots indicate SMFs. Data show mean ± SD (n=3).

Figure 1 continued on next page

Figure 1 continued

(**C**) UMAP from aggregated single cell RNA-seq shows expression of different phases of MuSCs (quiescent MuSCs, activated MuSCs and myoblasts), ECs (tip ECs and ECs) and from likely contaminant cells such as macrophages (Mφ) and smooth muscle cells (SMC). (**D**) UMAP from aggregated data visualized by sample day showing MuSCs segregated by the sample day but overlap in the EC population. Red dots indicate intact (day 0) and blue dots indicate 3 days following CTX. (**E**) Expression of quality control genes such as *eGFP*, *tdTomato*, *CreERT2,* and EC genes such as *Cdh5*, *Kdr,* and *Flt1*. (**F**) Genome browser tracks of whole muscle and TU-tagged MuSC nascent RNA (GSE97399, ***van Velthoven et al., 2017***). *Kdr* and *Pecam1* expression can be found in the MuSC fraction. As control, *Myh1* is highly expressed in the whole muscle preparation but largely absent in the MuSC fraction. *Sdc4* and *Calcr* are highly expressed in MuSC and less so in the whole muscle fraction. (**G**) qPCR for *Kdr, Flt1, Nrp1* and *Nrp2* in EC lines (bEnd.3 and C166), muscle cell line (C2C12) and MuSC-derived myoblasts in growth and differentiation medium (DM) shows low level expression of VEGFRs and VEGF co-receptors. Data show mean ± SD (n=3). (**H**) RNAScope of *Flt1* on freshly isolated single muscle fibers from *Pax7*^{tdT} mice shows *Flt1* expression (green) and tdTomato (red) in MuSCs. Nuclei were counterstained with DAPI (blue). Scale bar indicates 5 µm. (**I**) Immunostaining for PECAM1, VE-cadherin (VE-Cad), VEGFA co-receptors (NRP1 and NRP2) and VEGFA receptors (FLT1 and FLK1) in bEnd.3 EC cell line and MuSC-derived myoblasts (MB). Nuclei were counterstained with DAPI (blue). Scale bar indicates 20 µm.

The online version of this article includes the following source data and figure supplement(s) for figure 1:

Source data 1. Measurement of EC gene signal including VEGF receptor genes in MuSCs.

Figure supplement 1. EC gene signal in MuSCs.

Figure supplement 1—source data 1. Measurement of EC gene signal in MuSCs.

supplement 1L). We noticed that EC prototypic markers such as *Flt1* are broadly expressed with small amounts in MuSCs. Complementary data from different laboratories showed the clear expression of EC prototypic markers such as *Cdh5*, *Flt1,* and *Kdr*, using microarrays and Bulk-RNA-seq (***Figure 1—figure supplement 1A and B***; ***Fukada et al., 2007***; ***Ryall et al., 2015***). RNA-seq data from fixed quiescent, early activated and late activated MuSCs show that *Flt1* may be transiently upregulated during the early activation process (***Figure 1—figure supplement 1C***; ***Yue et al., 2020***). To confirm whether the EC gene mRNAs were transcribed from MuSCs, we utilized previously published MuSC nascent RNA transcriptome from TU-tagged samples (***Gay et al., 2013***; ***van Velthoven et al., 2017***). As expected, *Myh1* was represented in the whole muscle but was absent in the TU-tagged MuSCs (***Figure 1F***), indicating that the nascent MuSCs were devoid of cellular contamination from other cells in the muscle. Inversely, the nascent MuSC transcript was over-represented for MuSC related genes such as *Calcr* and *Sdc4*. Interestingly, we were able to detect EC genes such as *Kdr* and *Pecam1* in the TU-tagged MuSC samples indicating that they were actively transcribed by MuSCs (***Figure 1F***, ***Figure 1—figure supplement 1D***).

We also verified the expression of *Vegfr* genes (*Kdr*, *Flt1*, *Nrp1,* and *Nrp2*) in MuSCs using RT-qPCR (***Figure 1G***). In addition, we verified the expression of *Flt1* by performing in situ hybridization using RNAScope on MuSC on whole muscle fiber, which we currently believe to be the gold standard for expression studies (***Figure 1H***). Finally, in MuSC-derived myoblasts, NRP1and NRP2 expression was detectable with comparable intensity compared with EC cell line, while FLT1 expression was detectable with lower intensity compared with EC cell line (***Figure 1I***). By contrast, PECAM1, VE-Cadherin and FLK1 expression, which was clearly detected in EC cell line, was undetectable level in myoblasts. Taken together, these data indicate that there are both transcripts of these EC canonical genes and EC canonical proteins in MuSCs.

VEGFA induces proliferation and cell survival but not differentiation in myoblasts

Since VEGFRs were expressed in MuSCs in small amounts and their ligand, VEGFA, was highly expressed in MuSCs (***Verma et al., 2018***), we wanted to investigate whether there were any biological effects to induction by VEGFA. We found that treatment with VEGFA could increase proliferation of MuSC-derived myoblasts at low dose but inhibit proliferation at high dose of VEGFA, a phenomenon that has been previously described in ECs (***Noren et al., 2016***; ***Figure 2—figure supplement 1A***). We saw no effect on differentiation by VEGFA as evaluated by myosin heavy chain (MyHC) staining, fusion index and RT-qPCR (***Figure 2—figure supplement 1B–D***). By contrast, crystal violet staining showed that VEGFA could significantly increase survival as judged by number of myoblasts following UV-mediated apoptotic cell death induction (***Figure 2—figure supplement 1E and F***). To investigate apoptosis

in detail, we optimized Annexin V assay following thapsigargin-mediated endoplasmic reticulum (ER)-stress (**Hirai et al., 2010**) so that we could study deviation at ~ED50 while still performing experiments to remove the confounding variable to proliferation from the experimental setup (**Figure 2—figure supplement 1G and H**). We had previously shown that MuSCs are the predominant cells that secrete VEGFA in skeletal muscle (**Verma et al., 2018**) and while adding exogenous VEGFA did not improve cell survival, blocking VEGFA via a soluble form of FLT1-FC increased the number of apoptotic and necrotic myoblasts in vitro (**Figure 2A and B**).

VEGFA-facilitated cell survival in MuSC-derived myoblasts is mediated through FLT1

To characterize the VEGF receptor responsible for the anti-apoptotic effect of VEGFA on MuSC-derived myoblasts, we used pharmacological inhibitors of the VEGF receptors (**Figure 2C and D**). We used blocking antibody for the VEGF receptors FLT1 (anti-FLT1 antibody), small molecule inhibitors for FLK1 (SU4502 and ZM306416) and the FLK1 co-receptor NRP1 (EG00229) following thapsigargin induction (**Figure 2A and D**). Surprisingly, inhibiting FLK1, the major signaling RTK for VEGFA, had no effect on myoblasts survival following thapsigargin induction (**Figure 2D**). By contrast, blocking FLT1 via blocking antibody greatly decreased the survival of myoblasts following thapsigargin induction (**Figure 2D**). To confirm this interesting result using genetic tools, we obtained myoblasts with *Pax7-CreER*-inducible deletion of *Flt1* mice (*Pax7*$^{+/CreER}$:*Flt1*$^{Loxp/Loxp}$ or MuSC-*Flt1*$^{\Delta/\Delta}$) and the control mice (*Pax7*$^{+/+}$:*Flt1*$^{Loxp/Loxp}$). In vitro 4-OHT-mediated genetic deletion of *Flt1* (MuSC-*Flt1*$^{\Delta/\Delta}$) resulted in down-regulation of *Flt1* RNA and FLT1 protein expression (**Figure 2—figure supplement 1I and J**), and increased spontaneous apoptotic cell death even without induction of apoptosis (**Figure 2E**). By contrast, *Flt1* deletion did not affect cell proliferation assessed by EdU staining or myogenic differentiation assessed by MyHC staining (**Figure 2—figure supplement 1K–M**). When thapsigargin-induced apoptosis was induced, the MuSC-*Flt1*$^{\Delta/\Delta}$ myoblasts had increased apoptosis that was not responsive to exogenous VEGFA (**Figure 2F**).

AKT1 signaling is involved in apoptosis of muscle stem cells

VEGFA signaling is mediated through Extracellular signal-Regulated Kinase (ERK), p38 Mitogen-Activated Protein Kinase (MAPK), and Protein kinase B (AKT1). In ECs, VEGFA is known to protect cells from apoptosis via AKT1 (**Domigan et al., 2015**; **Lee et al., 2007**). However, it is not known whether VEGFA can similarly activate AKT1 in MuSC-derived myoblasts. While the role of AKT1 has been explored in proliferation and differentiation in myoblasts, its role in apoptosis has not been well characterized (**Loiben et al., 2017**). We assessed for AKT1 activation via phosphorylated AKT1 (pAKT1) in MuSC-derived myoblasts. We found that exogenous VEGFA could induce AKT1 phosphorylation (pAKT1) (**Figure 2G and H**, **Figure 2—figure supplement 1N and O**). This response was blunted in MuSC-*Flt1*$^{\Delta/\Delta}$ myoblasts and was no longer responsive to VEGFA (**Figure 2G and H**, **Figure 2—figure supplement 1N and O**). Lastly, we wanted to confirm that AKT1 activation could improve myoblast survival. We infected lentiviral *E4ORF1* or *MyrAKT1* vectors in myoblasts, both of which gene products have been shown to specifically activate AKT1 without activating ERK or p38 (**Kobayashi et al., 2010**). We found that overexpression of either of these genes improved cell survival compared with the control in vitro following induction of apoptosis via thapsigargin (**Figure 2I**). These data establish FLT1-AKT1 as the cascade linking VEGFA to apoptosis in MuSC-derived myoblasts during muscle regeneration (**Figure 2J**).

VEGFA-FLT1 pathway protects MuSCs from apoptosis in vivo

Endogenous and exogenous VEGFA have been shown to regulate cell survival and protect ECs from apoptosis (**Gerber et al., 1998**; **Lee et al., 2007**). To assess whether additional VEGFA had an effect on MuSC behaviors in vivo, we used mice carrying the *Vegfa*$^{+/Hyper}$ allele for injury-mediated TA muscle regeneration following $BaCl_2$ injection (**Figure 3A and B**; **Miquerol et al., 1999**). MuSC-derived myoblasts from *Pax7*$^{+/tdT}$:*Vegfa*$^{+/Hyper}$ mice showed around 2.8-fold increased expression of *Vegfa* but not the *Vegfr* genes compared with myoblasts from wild-type mice (**Figure 3—figure supplement 1A**). Interestingly, while treatment with VEGFA alone had no effect on apoptosis in vitro, the MuSCs from *Pax7*$^{+/tdT}$:*Vegfa*$^{+/Hyper}$ mice showed decreased cell death in regenerating muscle by 1 day following $BaCl_2$ injection (**Figure 3C**). Consequently, single muscle fibers from *Pax7*$^{+/tdT}$:*Vegfa*$^{+/Hyper}$

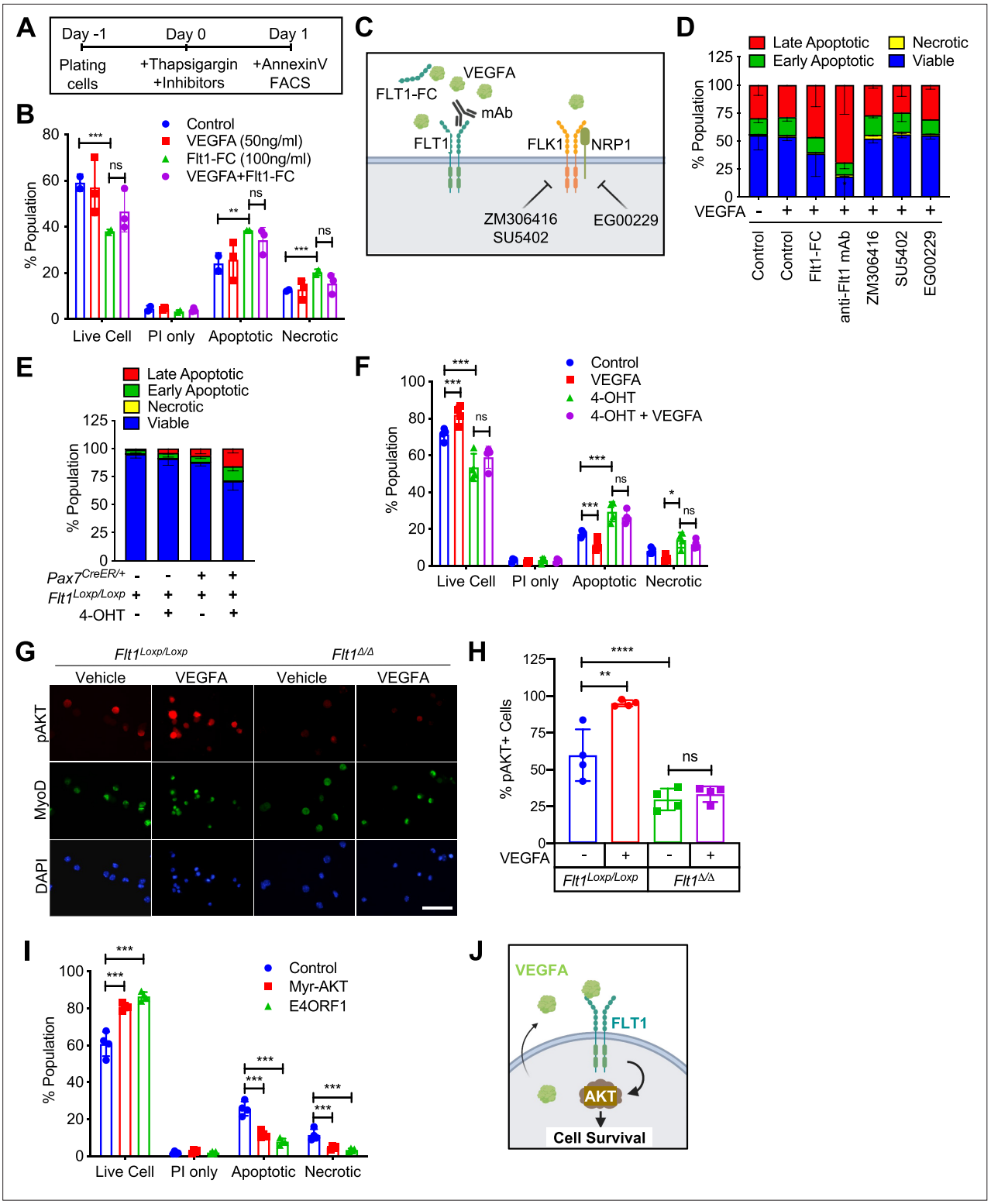

Figure 2. VEGFA-FLT1-AKT1 axis controls apoptosis in MuSC in vitro. (**A**) Experimental scheme for assessing apoptosis following thapsigargin induction in myoblast culture. (**B**) Decreased cell survival in myoblast in vitro as VEGFA is blocked using 100 ng/ml FLT1-FC (a VEFGA trap) following thapsigargin induction. This phenotype is partially rescued with exogenous VEGFA (50 ng/ml). Data show mean ± SD (n=3). (**C**) Graphical representation of the various tools used to interrogate the VEGFA pathway in this figure. This panel created with BioRender.com, and published using a TQ26O8B2M7 license with permission. (**D**) Following thapsigargin induction, apoptotic and necrotic cells are increased with inhibition of FLT1 via FLT1-FC or anti-FLT1 antibody (anti-FLT1 mAb) but not FLK1 (SU5402 and ZM306416) or NRP1-FLK1 inhibition (EG00229) following exogenous VEGFA (50 ng/ml). Data show

Figure 2 continued on next page

Figure 2 continued

mean ± SD (n=3). (**E**) 4-OHT induced deletion of *Flt1* in *Pax7*$^{+/CreER}$:*Flt1*$^{Loxp/Loxp}$ myoblasts is sufficient to reduce cell survival in myoblast without induction of apoptosis. Data show mean ± SD (n=3). (**F**) Cell survival is decreased in vitro in myoblast with thapsigargin induction following 4-OHT mediated deletion of *Flt1* in *Pax7*$^{+/CreER}$:*Flt1*$^{Loxp/Loxp}$ myoblast that is not rescued by exogenous VEGFA. Blue indicates MuSC-*Flt1*$^{+/+}$, red indicates MuSC-*Flt1*$^{+/+}$ with 50 ng/ml VEGFA, green indicates MuSC-*Flt1*$^{Δ/Δ}$ and purple indicates MuSC-*Flt1*$^{Δ/Δ}$ with 50 ng/ml VEGFA. Data show mean ± SD (n=3). (**G**) Representative images of pAKT1 (red) in myoblast stained by MyoD (green) in MuSC-*Flt1*$^{+/+}$ and MuSC-*Flt1*$^{Δ/Δ}$ myoblasts induced with exogenous VEGFA. Nuclei were counterstained with DAPI (blue). Scale bar indicates 50 µm. (**H**) Quantification of pAKT1 in myoblasts stained by MyoD in MuSC-*Flt1*$^{+/+}$ and MuSC-*Flt1*$^{Δ/Δ}$ myoblast induced w/wo exogenous VEGFA. VEGFA induction increases pAKT1 in MuSC-*Flt1*$^{+/+}$ myoblasts but this response is lost in MuSC-*Flt1*$^{Δ/Δ}$ myoblasts. Data show mean ± SD (n=3). (**I**) Annexin V quantification of myoblasts transfected with myr-AKT1 and E4ORF1 to activate AKT1 showed increased cell survival of myoblasts following thapsigargin induction. Data show mean ± SD (n=3). (**J**) Representative model for VEGFA-FLT1-AKT1 axis-mediated MuSC survival. This panel created with BioRender.com, and published using a TQ26O8B2M7 license with permission.

The online version of this article includes the following source data and figure supplement(s) for figure 2:

Source data 1. Measurement of VEGFA-FLT1-AKT1 axis for apoptosis in MuSC in vitro.

Figure supplement 1. VEGFA-FLT1-AKT1 axis for cell survival in MuSC in vitro.

Figure supplement 1—source data 1. Measurement of VEGFA-FLT1-AKT1 axis for cell survival in MuSC in vitro.

Figure supplement 1—source data 2. Uncropped blotting image of ***Figure 2—figure supplement 1N***.

mice showed increased number of MuSCs, compared with those from *Pax7*$^{+/tdT}$:*Vegfa*$^{+/+}$ mice by 28 days following $BaCl_2$ injection (***Figure 3D***). In addition, muscle regeneration was promoted in *Vegfa*$^{+/Hyper}$ mice in the early (14 days) and late (28 days) muscle repair processes as judged by fiber diameter and increase in eMHC(+) regenerating muscle fibers (***Figure 3E and F***, ***Figure 3—figure supplement 1B–F***,).

We then performed the reciprocal experiment to investigate the consequence of *Vegfa* loss in MuSCs in vivo, and utilized MuSC-specific *Vegfa* knockout mice (*Pax7*$^{+/CreER}$:*Vegfa*$^{Loxp/Loxp}$). We have previously shown that vasculature in the MuSC-*Vegfa*$^{Δ/Δ}$ mouse muscle is perturbed and the proximity between the MuSC and EC is increased (***Verma et al., 2018***). However, the functional consequences of this remained unknown. We confirmed that clear downregulation of VEGFA protein in MuSC-derived myoblasts isolated from MuSC-*Vegfa*$^{Δ/Δ}$ mice (***Figure 3—figure supplement 2A***). We noticed that deletion of *Vegfa* in MuSCs in the MuSC-*Vegfa*$^{Δ/Δ}$ mouse muscle led to an increase in the proportion of dead MuSCs following $BaCl_2$ injection (***Figure 3G***). Consequently, the number of MuSCs in the MuSC-*Vegfa*$^{Δ/Δ}$ muscle were significantly reduced following recovery after injury without difference in the MuSC numbers in MuSC-*Vegfa*$^{Δ/Δ}$ muscle at homeostasis (***Figure 3H***). In addition, the muscle had a regenerative defect as indicated by the shift in fiber size distribution, decrease in the size of regenerating eMHC(+) fiber and increased adipose following muscle injury (***Figure 3B, I and J***, ***Figure 3—figure supplement 2B–E***, ***Figure 3—figure supplement 1E and F***). While a limitation of this experiment is that the MuSC fusion into the fiber also deletes *Vegfa* from the fiber themselves, muscle-fiber-specific deletion of *Vegfa* has not shown an effect on fiber size (***Delavar et al., 2014***). These data indicate that cell intrinsic VEGFA improves cell survival of MuSCs and that loss of MuSC-derived VEGFA results in reduced muscle regeneration.

Since FLT1 but not FLK1 was detected in MuSCs and MuSC-derived myoblasts, we asked whether the *Flt1* had an effect on MuSC survival in vivo, we evaluated cell death in MuSCs from MuSC-*Flt1*$^{Δ/Δ}$ mouse muscle. We induced muscle regeneration using $BaCl_2$ for 1 day and assessed for cell death in MuSCs. As seen in vitro, we found that loss of *Flt1* in MuSCs (***Figure 2—figure supplement 1I and J***) resulted in increased cell death during early regeneration (***Figure 3K***). Consequently, single muscle fibers from MuSC-*Flt1*$^{Δ/Δ}$ mice showed a decreased number of MuSCs, compared with those from MuSC-*Flt1*$^{+/+}$ mice by 28 days following $BaCl_2$ injection (***Figure 3L***). We also examined the long-term in vivo consequence of deleting *Flt1* from MuSC. There was no significant muscle phenotype in MuSC-*Flt1*$^{Δ/Δ}$ muscle at homeostasis (***Figure 3B, M and N***). However, following injury, the MuSC-*Flt1*$^{Δ/Δ}$ muscle had a modest regenerative defect as indicated by the shift in fiber size distribution following muscle injury and decrease in size of eMHC(+) regenerating fibers (***Figure 3B, M and N***, ***Figure 3—figure supplement 2F–J***, ***Figure 3—figure supplement 1E and F***).

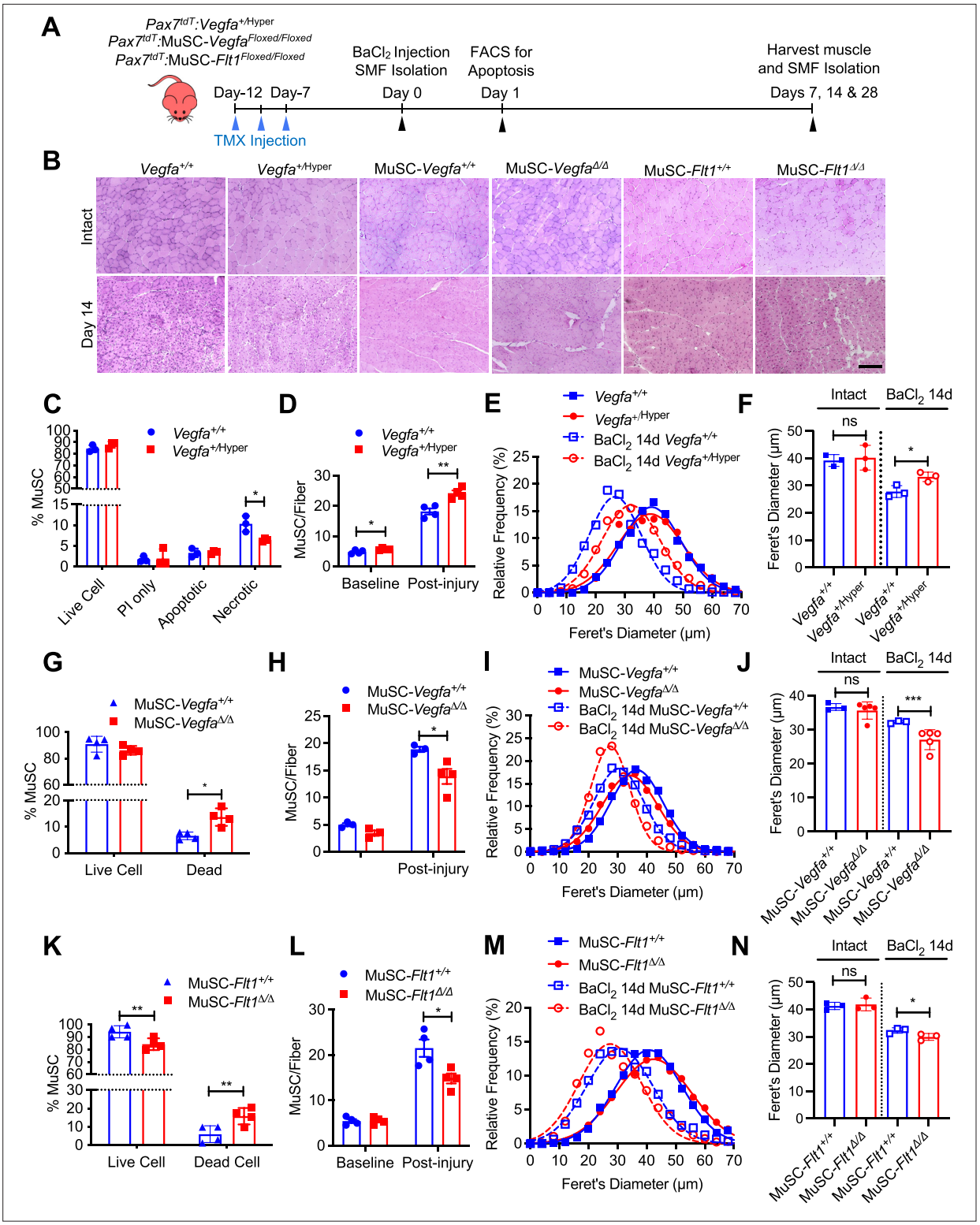

Figure 3. MuSC-derived *VEGFA* and *Flt1* requires proper skeletal muscle regeneration. (**A**) Experimental schema detailing the experiments performed in this figure. The *Pax7*$^{+/CreER}$:*R26R*^{tdT}:*Vegfa*$^{+/Hyper}$ (*Vegfa*$^{+/Hyper}$) *Pax7*$^{+/CreER}$:*R26R*^{tdT}:*Vegfa*$^{Loxp/Loxp}$ *for* MuSC-*Vegfa*$^{\Delta/\Delta}$ and *Pax7*^{tdT}:*Flt1*$^{Loxp/Loxp}$ for MuSC-*Flt1*$^{\Delta/\Delta}$ lines were pulsed with tamoxifen (TMX) prior to $BaCl_2$-induced muscle injury followed by investigations. (**B**) Representative H&E-stained images for intact and on 14-day post injury TA muscle from MuSC-*Vegfa*$^{+/Hyper}$, MuSC-*Flt1*$^{\Delta/\Delta}$ *and* MuSC-*Vegfa*$^{\Delta/\Delta}$ mice and their representative controls. Scale bar indicates 100 μm. (**C**) Annexin V staining show less necrotic cells in MuSC from *Vegfa*$^{+/Hyper}$ mice compared with the control one day following injury. Data show mean ± SD (n=3). (**D**) Quantification of MuSCs from single muscle fibers show increased Pax7 immunofluorescence positive MuSCs in *Vegfa*$^{+/Hyper}$ EDL

Figure 3 continued on next page

Figure 3 continued

muscle compared with the control mice at base line and 14 days post injury. Data show mean ± SD (n=4). (**E**) Fiber size distribution and (**F**) mean feret's diameter of uninjured and regenerating muscle 14 days post injury from *Vegfa*$^{+/Hyper}$ and control mice show no difference at baseline but an increase in fiber diameter following injury. Data show mean ± SD (n=3). (**G**) Annexin V staining show increased dead cells in MuSCs from MuSC-*Vegfa*$^{\Delta/\Delta}$ mice one day following $BaCl_2$ compared with the control MuSC-*Vegfa*$^{+/+}$ mice. Data show mean ± SD (n=4). (**H**) Quantification of MuSCs from single muscle fiber at base line and 14 days post injury shows no difference at baseline and reduced MuSC numbers at 14 days. Data show mean ± SD (n=4). (**I**) Fiber size distribution and (**J**) mean feret's diameter of uninjured and regenerating muscle 14 days post injury from MuSC-*Vegfa*$^{\Delta/\Delta}$ and MuSC-*Vegfa*$^{+/+}$ mice show no difference at baseline but a decrease in fiber diameter following injury. Data show mean ± SD (n=3 or 5). (**K**) Annexin V staining show increased apoptosis in MuSCs from MuSC-*Flt1*$^{\Delta/\Delta}$ mice one day following injury compared with the control MuSC-*Flt1*$^{+/+}$ mice. Data show mean ± SD (n=4). (**L**) Quantification of MuSCs from single muscle fiber show decreased MuSCs in MuSC-*Flt1*$^{\Delta/\Delta}$ EDL muscle at base line and 14 days post injury compared with the control MuSC-*Flt1*$^{+/+}$ mice. Data show mean ± SD (n=4). (**M**) Fiber size distribution and (**N**) mean feret's diameter of uninjured and regenerating muscle from MuSC-*Flt1*$^{\Delta/\Delta}$ and compared with the control MuSC-*Flt1*$^{+/+}$ mice show no difference at baseline but a decrease in fiber diameter following injury. Data show mean ± SD (n=3).

The online version of this article includes the following source data and figure supplement(s) for figure 3:

Source data 1. Measurement of MuSC-derived VEGFA and Flt1 for proper skeletal muscle regeneration.

Figure supplement 1. MuSC-derived VEGFA and Flt1 for skeletal muscle regeneration.

Figure supplement 1—source data 1. Mesurement of MuSC-derived VEGFA and Flt1 for skeletal muscle regeneration.

Figure supplement 2. MuSC-derived VEGFA and Flt1 regulating skeletal muscle regeneration.

Figure supplement 2—source data 1. Measurement of MuSC-derived VEGFA and Flt1 during skeletal muscle regeneration.

VEGFA-FLT1 pathway regulates muscle pathology in DMD model mice

While angiogenic defects have been reported in the *mdx* mice as well as in golden retrieval muscular dystrophy (GRMD; canine model of DMD) (***Verma et al., 2010***; ***Latroche et al., 2015***; ***Verma et al., 2019***; ***Kodippili et al., 2021***; ***Podkalicka et al., 2021***), it is not clear whether VEGF family and its receptors are implicated in human dystrophinopathies. We probed the VEGF ligands and receptors in microarrays (***Supplementary file 1***) from skeletal muscles and MuSCs from *mdx* mice (***Tseng et al., 2002***; ***Pallafacchina et al., 2010***) and skeletal muscles from the GRMD (***Vieira et al., 2015***). *Vegfa* was downregulated in both models (***Figure 4—figure supplement 1A***). *Flt1* was also downregulated in GRMD but not *mdx* muscles. To examine whether VEGF signaling is altered in DMD patients, we performed gene expression analysis on previously available data from microarrays from patients with DMD (***Chen et al., 2000***). We also aggregated and probed microarray data from muscle biopsies of patients with various neuromuscular diseases or of healthy individuals after exercise (***Bakay et al., 2006***). In the microarray data, *Vegfa* expression was increased after an acute bout of exercise, and *Vegfa* expression was reduced in ALS muscle, BMD muscle, as well as both early and late phases of DMD muscle (***Figure 4—figure supplement 1A***). These data indicate that *Vegfa* expression is decreased in dystrophinopathy, and thus increasing VEGFA may be a therapeutic target for DMD.

Therefore, we crossed the MuSC-*Flt1*$^{\Delta/\Delta}$ mice with the chronically regenerating DMD model mice (*mdx*) to generate *mdx*:MuSC-*Flt1*$^{\Delta/\Delta}$ mice, and analyzed long-term effects of *Flt1* deletion (***Figure 4A***, ***Figure 4—figure supplement 1B and C***). Importantly, we found a significant decrease in fiber diameter, increased fibrosis and CD31(+) capillary density (***Figure 4B–D***, ***Figure 4—figure supplement 1C and D***) in TA muscle. This was accompanied by a physiological decrease in muscle perfusion as shown by laser Doppler flow at 12 months (***Figure 4E***) as well as a functional decline in muscle strength as judged by grip strength both acutely and chronically (***Figure 4F***).

By contrast, when we crossed the *Vegfa*$^{+/Hyper}$ mice with *mdx* mice (***Figure 4A***), we noticed a significant increase in fiber diameter, increase in capillary density and decreased fibrosis (***Figure 4G–I***, ***Figure 4—figure supplement 1D–F***) in both TA and diaphragm muscle of *mdx:Vegfa*$^{+/Hyper}$ mice. This was accompanied by a physiological increase in muscle perfusion as shown by laser Doppler flow at 12 months age (***Figure 4J***) as well as a functional increase in muscle strength as judged by grip strength (***Figure 4K***) without a change in body mass (***Figure 4—figure supplement 1E***). Lastly, when the muscle was injured acutely, with $BaCl_2$, the *Vegfa*$^{+/Hyper}$ mouse had lower number of apoptotic MuSC (***Figure 4—figure supplement 2A–C***). These data indicate that VEGFA-FLT1 axis is a therapeutic target for the pathology seen in the DMD model *mdx* mice.

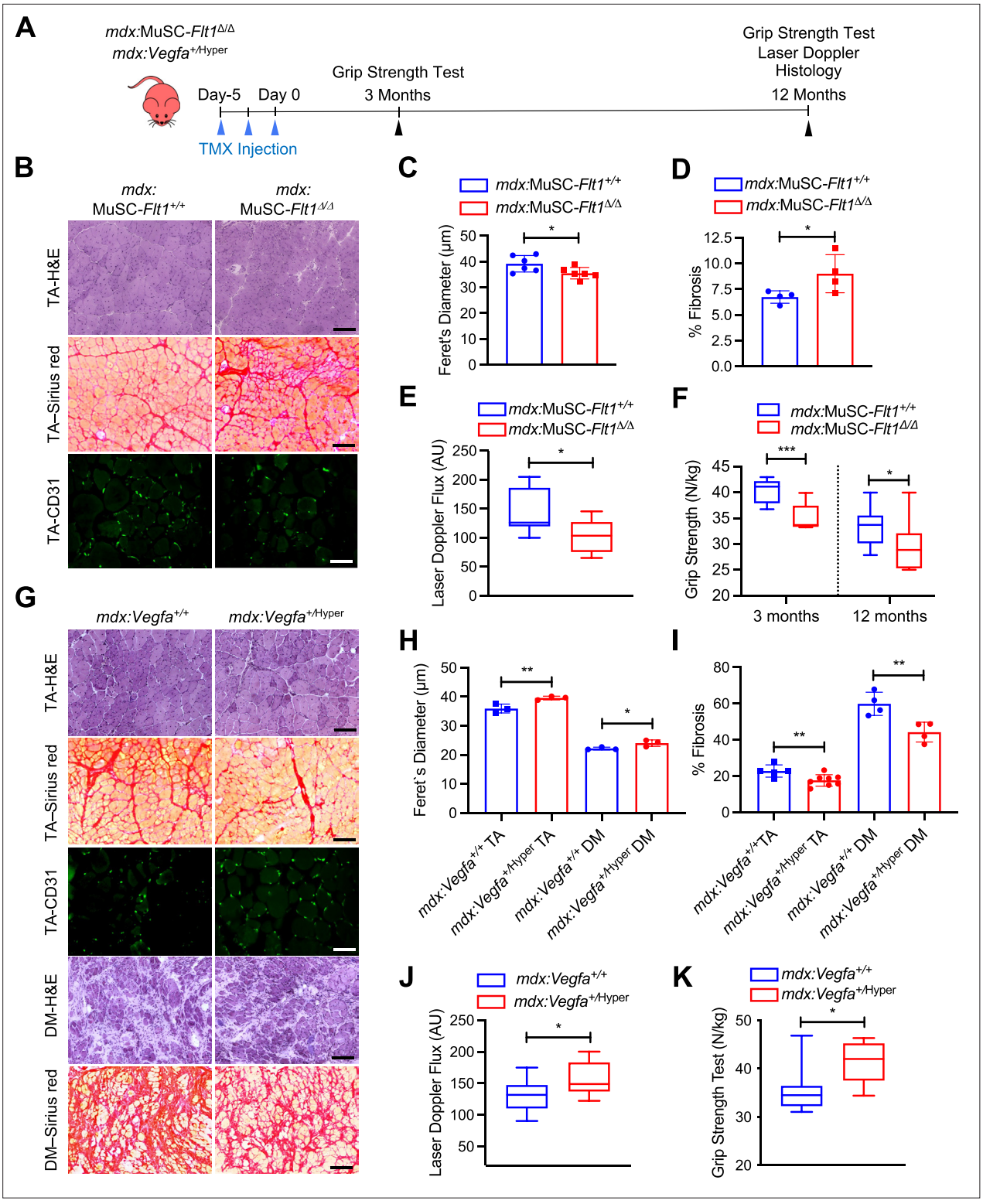

Figure 4. VEGFA-FLT1 pathway in MuSCs regulates muscle pathology in DMD model mice. (**A**) Experimental schema detailing the experiments performed in this figure. The *mdx:Pax7*^{tdT}*:Flt1*$^{Loxp/Loxp}$ was pulsed with tamoxifen (TMX) to generate *mdx*:MuSC-*Flt1*$^{\Delta/\Delta}$ mice prior to investigation. *mdx:Vegfa*$^{+/Hyper}$ mouse line was used without any induction. (**B**) Representative H&E (scale bar, 100 μm), Sirius red staining (red; scale bar, 100 μm) and CD31(+) capillaries (green; scale bar, 25 μm) from *mdx*:MuSC-*Flt1*$^{+/+}$ and *mdx*:MuSC-*Flt1*$^{\Delta/\Delta}$ mouse TA muscle at 3 months of age. (**C**) Smaller average fiber size in *mdx*:MuSC-*Flt1*$^{\Delta/\Delta}$ compared with the control *mdx*:MuSC-*Flt1*$^{+/+}$ mouse TA muscle. Data show mean ± SD (n=6). (**D**) Increased fibrotic area in *mdx*:MuSC-*Flt1*$^{\Delta/\Delta}$ compared with the control *mdx*:MuSC-*Flt1*$^{+/+}$ mouse TA muscle. Data show mean ± SD (n=4). (**E**) Decreased muscle perfusion

Figure 4 continued on next page

Figure 4 continued

in *mdx*:MuSC-*Flt1*$^{\Delta/\Delta}$ compared with the control *mdx*:MuSC-*Flt1*$^{+/+}$ mouse TA muscle. Data show mean ± SD (n=3). (n=3). (**F**) Decreased grip strength normalized to body weight in *mdx*:MuSC-*Flt1*$^{\Delta/\Delta}$ compared with the control *mdx*:MuSC-*Flt1*$^{+/+}$ mouse TA muscle at both 3 and 12 months of age. Data show mean ± SD (n=3). (**G**) Representative H&E (scale bars, 100 µm), Sirus red stain staining (red; scale bars, 100 µm) and CD31(+) capillaries (green; scale bar, 25 µm) from TA muscle of *mdx:Vegfa*$^{+/Hyper}$ and *mdx:Vegfa*$^{+/+}$ mouse at 3 months. (**H**) Increased average fiber size in *mdx:Vegfa*$^{+/Hyper}$ compared with the control *mdx:Vegfa*$^{+/+}$ mouse TA and diaphragm (DM) muscle. Data show mean ± SD (n=3). (**I**) Decreased fibrosis in *mdx: Vegfa*$^{+/Hyper}$ compared with the control *mdx:Vegfa*$^{+/+}$ mouse TA muscle and diaphragm (DM) muscle. Data show mean ± SD (n=4 to 8). (**J**) Muscle perfusion is increased in *mdx:Vegfa*$^{+/Hyper}$ compared with the control *mdx:Vegfa*$^{+/+}$ mouse TA muscle. Data show mean ± SD (n=3). (**K**) Grip strength normalized to body weight is increased in *mdx:Vegfa*$^{+/Hyper}$ compared with the control *mdx:Vegfa*$^{+/+}$ mice. Data show mean ± SD (n=3).

The online version of this article includes the following source data and figure supplement(s) for figure 4:

Source data 1. Measurement of VEGFA-FLT1 pathway in MuSCs for muscle pathology in DMD model mice.

Figure supplement 1. VEGFA-FLT1 pathway in MuSCs for muscle pathology in DMD model mice.

Figure supplement 1—source data 1. Measurement of VEGFA-FLT1 pathway in MuSCs for muscle pathology in DMD model mice.

Figure supplement 2. VEGFA-FLT1 pathway in MuSCs regulates apoptotic cell death in DMD model mice.

Figure supplement 2—source data 1. Measurement of apoptotic cell death.

Discussion

In this report, we performed bulk and single cell RNA sequencing on MuSCs and ECs. Since deep reads can significantly reduce the effect of the technical noise in scRNA-seq, it can improve estimation of minor transcriptional state of a given cell (***Zhang et al., 2020***). Unexpectedly, we found that MuSCs broadly express EC prototypic markers in small amounts and used multiple different bioinformatics techniques to validate the results. While similar phenomenon in myogenic cells during development and existence of blood-vessel-associated myoendothelial cells in the adult skeletal muscle have been previously described, no functional follow up as been performed leading to the questions whether these minor expression profiles were artifacts or functional (***De Angelis et al., 1999***; ***Minasi et al., 2002***; ***Tamaki et al., 2002***; ***Zheng et al., 2007***; ***Roobrouck et al., 2011***; ***Huang et al., 2014***; ***Charville et al., 2015***; ***Goel et al., 2017***; ***Giordani et al., 2019***). Our goal was to see whether this small expression pattern had biological consequences. We ultimately decided to use *Flt1* for further investigations and used RNAscope and immunostaining to validate its expression in MuSCs. We found that *Flt1* indeed exerts a biological function even at a low expression. Signaling through VEGFA-FLT1-AKT1 can improve cell survival in MuSCs both in vivo and in vitro.

On a grander scale, our finding of EC prototype markers expressed in MuSC calls into two questions (1) the genes that we used to specify cellular identities and (2) the cellular identity of MuSCs and ECs. The former is important as when we experimentally label, induce or perform Cre-mediated gene knockout experiments based on our assumptions of different gene expression results which may be confounded for these low expressing genes. For example, we have previously investigated both *Flt1* and *Kdr* in mouse muscle using three different reporters and found them to be negative in MuSCs, thereby disregarding their cell-autonomous effect when evaluating global knockouts (***Verma et al., 2010***; ***Verma et al., 2018***). It is also possible that EC mRNAs are results of transcription from the cell or a result of mRNA transfer from neighboring cells (***Desrochers et al., 2016***). Of note, the transmission of *tdTomato* mRNA and protein from *Pax7*$^{+/CreERT2}$*:R26R*$^{+/tdT}$mice used in this study has been recently shown via exosome, opening up the possibility of transmission of other mRNA from MuSC to ECs (***Murach et al., 2020***). The later is an interesting phenomenon form a developmental point of view. MuSCs and ECs arise from a bipotent progenitor originated from somites during early development (***Kardon et al., 2002***; ***Hutcheson and Kardon, 2009***; ***Lagha et al., 2009***; ***Mayeuf-Louchart et al., 2014***; ***Mayeuf-Louchart et al., 2016***). Therefore, it is possible that there is a permissive chromatin state that allows for expression of reciprocal genes in the two populations. Along the lines of these observations, FLK1(+) or VE-cadherin(+) cells can contribute to myogenic cells in vitro and after cell transplantation (***Tamaki et al., 2002***; ***Le Grand et al., 2004***; ***Zheng et al., 2007***; ***Huang et al., 2014***), and during development (***Motoike et al., 2003***; ***Mayeuf-Louchart et al., 2014***; ***Drummond and Hatley, 2018***). Important notion is that the PDGFRα(-)FLK1(+) population exhibited restricted potential to differentiate into the MuSCs in injured muscle (***Sakurai et al., 2008***). Interestingly, in the zebrafish, exogenous expression of *Etv2* in the fast muscle can lead to transdifferentiation of muscle fibers into functional vessels so there is evidence of cell fate flexibility (***Veldman et al., 2013***). The

potential of EC transdifferentiation was also examined by ETV2 overexpression in five human cell types, skeletal muscle cells, adipose-derived mesenchymal stem cells, umbilical-cord-derived mesenchymal stem cells, embryonic lung fibroblast cells, and skin fibroblast cells. Among them, human skeletal muscle cells showed the highest amenability for this EC induction following infection with ETV2 lentivirus vector (**Yan et al., 2019**). Conversely, *Etv2*-deficient vascular progenitors can differentiate into skeletal muscle cells (**Chestnut et al., 2020**). It would be interesting to see whether other EC gene signatures also have functional consequences in the MuSC or muscle at large.

We decided to focus on function of *Flt1* among several EC genes expressed in MuSCs for further investigations on MuSC biology. Our pharmacological and genetic analyses demonstrate that MuSC-derived VEGFA has a drastic effect on cell survival in the via its receptor FLT1 by signaling through AKT1. While VEGFA binds to both FLT1 and FLK1, VEGFB and PGF only bind to FLT1. This creates a scenario where PGF and VEGFB binding can sequester FLT1, increasing free VEGFA availability for VEGFA-FLK1 binding which is the major VEGF signaling pathway for many cell types (**Vempati et al., 2014**). While PGF is not normally expressed in adult tissues, VEGFB is expressed in the MuSCs and muscle fiber (data not shown). Importantly, the VEGFB-FLT1 axis has also been shown to inhibit apoptosis in retina and brain cells in mouse models of ocular neurodegeneration and stroke (**Li et al., 2008**). While our results cannot rule out the involvement of VEGFB in protection of MuSC apoptosis, we provide evidence from both pharmacological and genetic data to indicate that VEGFA is involved.

Despite drastic effect of VEGFA-FLT1 on apoptosis in vitro, the long-term consequences of in vivo deletion of *Flt1* in the MuSC compartment were modest compared with deletion of *Vegfa* in the MuSCs unless crossing with *mdx* mice. Although *Vegfa* is required for both MuSC survival and recruitment of vascular niche (**Verma et al., 2018**), in the steady state, the MuSC turnover may be low enough that the apoptotic stress burden is low. We demonstrated that VEGFA improves cell survival during the proliferative stage following injury in *mdx:Vegfa*$^{+/Hyper}$ mice. The evidence that MuSC survival is impaired comes indirectly from transplantation experiments where MuSCs obtained from *mdx* mice engraft to a much lesser degree than those from WT mice (**Boldrin et al., 2015**).

During the review process of this paper, two additional labs reported complementary findings about VEGFA signaling in MuSC (**Chen et al., 2022**; **Groppa et al., 2023**). Groppa et al performed extensive transcriptomics to show role of the VEGFA system in muscle regeneration. They showed that VEGFA is expressed in expression in MuSC and inflammatory cells. In addition, VEGFA increased MuSC proliferation through KDR (FLK1). They also found that deletion of MuSC derived VEGFA lead to an increase in TUNEL(+) apoptotic MuSC. The role of KDR in MuSC was also corroborated by Chen et.al who showed that MuSC lacking KDR showed asymmetrical division deficits and limit MuSC proliferation resulting in impaired tissue regeneration. While both these reports focus on the role of VEGFA-KDR on proliferation, the current paper focuses on the role of VEGFA-FLT1 on MuSC survival.

VEGFA and FLT1 targeted therapies are being explored as both pro- and anti-angiogenic therapies for several indications including retinal degeneration, cancer, pre-eclampsia, and neuromuscular diseases (**Bae et al., 2005**; **Verma et al., 2010**; **Mac Gabhann et al., 2010**; **Keifer et al., 2014**; **Verma et al., 2019**; **Bosco et al., 2021**; **Xin et al., 2021**). As these therapies mature, it will be important to ascertain the MuSC-specific effects of VEGFA and FLT1.

Materials and methods

Mice

Flt1$^{LoxP/LoxP}$ were obtained from Gua-Hua Fong (**Ho et al., 2012**). *B6.Cg-Pax7*$^{tm1(cre/ERT2)Gaka/J}$ (*Pax7*$^{+/CreERT2}$; JAX stock# 017763; **Murphy et al., 2011**), *B6.Cg-Gt(ROSA)*$^{26Sortm9(CAG-tdTomato)Hze/J}$ (*Ai9*; JAX stock # 007909; **Madisen et al., 2010**), *Vegfa*$^{+/Hyper}$ (*Vegfatm1.1Nagy/J*; JAX stock# 027314; **Miquerol et al., 1999**) and *B6Ros.Cg-Dmd*$^{mdx-5cv}$*/J* (*mdx*^{5cv}; JAX stock #002379; **Chapman et al., 1989**) were obtained from Jackson Laboratory. *Kdr*$^{tm2.1Jrt/J}$ (*Flk1*$^{+/GFP}$) were obtained from Masatsugu Ema (**Ema et al., 2006**). *B6.Cg-Pax7*$^{tm1(cre/ERT2)Gaka/J}$ (*Pax7*$^{+/CreERT2}$) mice were crossed with the *B6.Cg-Gt(ROSA)*$^{26Sortm9(CAG-tdTomato)Hze/J}$ (*Ai9*) to yield the *Pax7*$^{+/CreERT2}$*:R26R*^{tdT}(*Pax7*^{tdT}) mice. *Pax7*^{tdT} mice were bred with the *Vegfa*$^{+/Hyper}$ and *Flk1*$^{+/GFP}$ to obtain *Pax7*$^{+/tdT}$*:Vegfa*$^{+/Hyper}$ and *Pax7*$^{+/tdT}$*:Flk1*$^{+/GFP}$ mice. *Vegfa*$^{LoxP/LoxP}$ mice obtained from Napoleone Ferrara (**Gerber et al., 1999**) were crossed with *Pax7*$^{+/CreERT2}$ to yield the *Pax7*$^{+/CreERT}$*:Vegfa*$^{LoxP/LoxP}$ mice. *Flt1*$^{LoxP/LoxP}$ mice obtained from Guo-Hua Fong (**Gerber et al., 1999**) were crossed with *Pax7*$^{+/CreERT2}$ to yield the *Pax7*$^{+/CreERT}$*:Flt1*$^{LoxP/LoxP}$ mice. Colonies for all the mice were established

in the laboratory. Cre recombination was induced using tamoxifen (T5648, MilliporeSigma) dosed as 75 mg/kg body weight x 3 times over 1 week at 3–6 weeks of age. Mice carrying the wild-type *CreERT2* allele were used for control experiments. TA muscle regeneration was induced by intramuscular injection of 20 µl of 1% $BaCl_2$ (342920, MilliporeSigma) or 20 µl of 10 µM Cardiotoxin (CTX) (V9125, MilliporeSigma). Mice used for this study is summarized in Key Resources Table.

Genotyping to detect the transgenic and mutant alleles was performed by PCR using the primers described on the web site of Jackson Laboratory shown in Key Resources Table. All primers were synthesized as custom DNA oligos from Integrated DNA technologies (IDT). Genotyping to detect the mutated allele of *mdx*^{5cv} was performed by PCR using the primers (0981 and 0982) shown in Key Resources Table. The PCR product DNA was digested with *Dra*III restriction enzyme (R3510S, New England Biolabs). Wild-type allele generated 180 bp and mutant allele generated 50 and 130 bp bands.

The animals were housed in an SPF environment and were monitored by the Research Animal Resources (RAR) of the University of Minnesota. All protocols (2204–39969A) were approved by the Institutional Animal Care and Usage Committee (IACUC) of the University of Minnesota and complied with the NIH guidelines for the use of animals in research.

Cell isolation by FACS

Pax7^{tdT}*:Flk1*^{GFP} mice were utilized for FACS-mediated MuSC and EC isolation as previously described (***Asakura et al., 2002***; ***Verma et al., 2018***). We performed extensive validation of the fluorescent reporter mice as previously described (***Figure 1—figure supplement 1A–C***; ***Verma et al., 2018***). Briefly, quiescent MuSCs and ECs were isolated from the hind limb skeletal muscle of 1- to 2-month-old *Pax7*^{tdT}*:Flk1*^{GFP} mice after digestion with collagenase type II. FACS was performed on an FACS sorter (BD FACSAria) and data were analyzed using FlowJo (BD Biosciences). Sorting gates, tdTomato(+) for MuSCs and GFP(+) for ECs, were strictly defined based on control cells isolated from wild-type mice and the forward scatter and side scatter gating. Sorted cells were immediately characterized by immunostaining on slide glasses, utilized for RNA preparation or cultured on collagen-coated plates in the myoblast growth medium as below to obtain MuSC-derived myoblasts and ECs. FACS analysis was performed as previously described (***Turaç et al., 2013***). Cells were either trypsinized (cultured cells) or a single cell suspension was obtained following enzymatic digestion as whole muscle-derived cells (***Asakura et al., 2001***; ***Asakura et al., 2002***). Cells were then washed with FACS buffer (2% BSA and 1 mM EDTA in PBS) followed by live/dead staining using ZombieNIR (423105, Biolegends). Cells were washed, then immunostained for cell surface markers. Blocking cells was performed with 1% BSA/PBS, and cells were incubated in fluorescently-conjugated antibody. FACS was performed on a Fortessa X-20 (BD Biosciences) with a 355 nm, 405 nm, 488 nm, 561 nm, and 640 nm lasers.

Cell culture

Mouse bEnd.3 EC cells (CRL-229), C166 EC cells (CRL-2581), and C2C12 myoblast cells (CRL-1772) were obtained from American Type Culture Collection (ATCC). Human 293 FT cells (R70007) were obtained from ThermoFisher Scientific. All cell lines were cultured in DMEM medium with 10% FBS, 100 units/ml of penicillin, and 100 µg of streptomycin at 37 °C in 5% O_2 and 5% CO_2. All cell lines were STR profiled to confirm their identity and tested negative for mycoplasma. MuSC-derived myoblast isolation from adult mice was performed as previously described (***Motohashi et al., 2014***). Briefly, after collagenase type II (CLS-2, Worthington) treatment, dissociated cells from mouse hindlimb muscle were incubated with anti-CD31-PE (12-0311-82, eBiosciences), anti-CD45-PE (12-0451-81, eBiosciences), anti-Sca1-PE (A18486, eBiosciences) and anti-Integrin α7 (ABIN487462, MBL International), followed by anti-PE microbeads (130-048-801, Miltenyi Biotec), and then performed LD column (130-042-901, Miltenyi Biotec) separation. Negative cell populations will be incubated with anti-Mouse IgG beads (130-048-402, Miltenyi Biotec), and then MS column (130-042-201, Miltenyi Biotec) separation was performed to isolate Integrin α7(+) MuSCs. MuSC-derived myoblasts were maintained in culture on collagen coated plates in myoblast medium containing 20% FBS, 20 ng/ml bFGF (PHG0263, Invitrogen), 100 units/ml of penicillin and 100 µg of streptomycin in HAM's-F10 medium. Cell cultures were maintained in a humidified incubator at 37 °C with 5% CO_2 and 5% O_2. 4-Hydroxy tamoxifen (4-OHT, H6278, MilliporeSigma) treatment (1 µM in EtOH) was used to induce *Flt1* deletion in myoblasts isolated from *Flt1*$^{LoxP/LoxP}$*:Pax7*^{CreERT2} mice. For cell survival assay,

1 x 10^5 cells were allowed to adhere for 1 day and starved overnight in 0.1% FBS in HAM's F10 medium. Then, cells were exposed to 1 µM EdU along with or without 2–100 ng/ml recombinant VEGFA (493 MV, R&D Systems) for 8 hr before being fixed and stained by the Click-iT EdU Alexa Fluor 488 Imaging Kit (C10337, Thermo Fisher Scientific). For induction of apoptosis in myoblasts, (1–2 x 10^5) cells were allowed to adhere to the plates for 16 hr. Thapsigargin-mediated apoptosis was induced by 1 µM of thapsigargin (T9033, MilliporeSigma) dissolved in EtOH with or without VEGFA, 100 ng/ml recombinant FLT1-FC (7756-FL, R&D Systems), 1 µg/ml anti-FLT1 monoclonal antibody (Angio-Proteomie, MAB7072), inhibitors of FLK1, 3 µM ZM306416 (2499/1, R&D Systems) and 10 µM of SU5402 (3300/1, R&D Systems) and an inhibitor of NRP1, 30 µM of EG00229 (6986/10, R&D Systems) for 24 hours. UV light-mediated apoptosis was induced by exposing the cells to UV light in cell culture hood for 45 s without medium. After UV exposure, cell survival was assessed 24 hr following culture in 0.1% FBS in HAM's F10 medium with or without VEGFA using the Crystal violet Assay Kit (ab232855, Abcam) and quantified the Crystal violet dye after solubilization by absorbance at 570 nm. To induce differentiation of myoblasts, the myoblast medium was replaced with differentiation medium that contained DMEM supplemented with 5% horse serum with or without VEGFA or bFGF for 1 or 3 days followed by anti-sarcomeric myosin heavy chain antibody (MF-20, Developmental Study Hybridoma Bank).

AKT1 induction

The lentiviral pCCL-E4ORF1 and pCCL-myrAkt1 constructs were a kind gift from Dr. Jason Butler (***Kobayashi et al., 2010***). A total of 293 FT cells (R70007, Thermo Fisher Scientific) were seeded in DMEM with 10% FBS and transfected with the lentivirus vectors along with pCMV-VSV-G (8454, Addgene), pRSV-Rev (12253, Addgene), and pMDLg/pRRE (12251, Addgene) using PolyJet transfection reagent (SL100688, Signagen Laboratories). The culture supernatant of the transfected 293 FT cells was added to MuSC-derived myoblast culture with 0.8 µg/ml polybrene (MilliporeSigma, H9268). pAKT1(+) cells were stained with anti-pAKT1 antibody (4060, Cell Signaling).

Western blotting

Protein extracts of MuSC-derived myoblast culture obtained with an NE-PER Nuclear and Cytoplasmic Extraction reagents (78833, Thermo Fisher Scientific) was used for western blotting. Protein concentration was determined by the Micro BCA Protein Assay Reagent kit (Thermo Fisher Scientific). Following electrophoresis, the proteins were transferred to an Immobilon P membrane (IPVH00010, EMD Millipore) overnight. pAKT1 was detected by Western blotting with anti-pAKT1 antibody (4060, Cell Signaling) followed by anti–rabbit IgG HRP (31460, Cell Signaling Technology). To verify equal loading proteins, the same blots were stripped and reprobed with anti-GAPDH HRP conjugated (3683, Cell Signaling) as a cytosolic marker. The reaction was developed using SuperSignal West Femto chemiluminescent substrate (PI37074, Fisher Scientific) in accordance with the manufacturer's instructions. Protein signals were detected and quantitated by iBright FL1500 (A44241, ThermoFisher Scientific).

Apoptosis assay

Apoptosis was measured using measured using Annexin V-Biotin Apoptosis Detection Kit (BMS500BT-100, eBioscience) as per the manufacture's instruction. Streptavidin-conjugated Alexa-Fluro-488 was used for detection. Propidium Iodide (PI) was used in all assays except when Pax7tdT(+) cells were utilized or when ZombieNIR (423105, Biolegends) was used. FACS was performed on a Fortessa X-20 (BD Biosciences) equipped with a 355 nm, 405 nm, 488 nm, 561 nm, and 640 nm lasers. For detection of apoptotic cells in TA muscle sections 3 days following $BaCl_2$ injection, TMX was injected into *mdx:Vegfa*$^{+/+}$*:Pax7*^{tdT} and *mdx:Vegfa*$^{+/Hyper}$*:Pax7*^{tdT} mice before $BaCl_2$ injection to label MuSCs during muscle regeneration. To detect apoptotic cells, the TA muscle sections were incubated with anti–activated caspase-3 antibody (ab214430, Abcam) followed by anti–rabbit Alexa-488 antibodies (A11008, ThermoFisher Scientific) for double immunostaining. DAPI (10236276001, MilliporeSigma) was used for counterstaining of nuclei. Microscopic images were captured by a DP-1 digital camera attached to BX51 fluorescence microscope with 10×, 20×or 40×UPlanFLN objectives with cellSens Entry 1.11 (all from Olympus).

Immunostaining of cells

Immunostaining for PECAM1, VE-Cadherin, VEGFA, VEGFRs was performed on collagen coated coverslips. Other immunostaining was performed on 35 mm tissue culture plates. Cells were fixed with 2% PFA for 5 min and immunostained as previously described (***Verma et al., 2010***). For membrane receptor staining, cells were permeabilized with 0.01% saponin (ICN10285525, ThermoFisher Scientific) which was kept in the staining solution until the primary antibodies were washed off. At which time, 0.01% Triton-X was added to all the buffers. The antibodies used for this study are listed in Key Resources Table.

Single muscle fiber isolation and staining

Extensor digitorum longus (EDL) muscle was dissected and digested with 0.2% collagenase type I (C0130, MilliporeSigma) for single muscle fiber isolation as previously described (***Verma et al., 2010***). Single muscle fibers were fixed with 2% PFA/PBS, permeabilized with 0.2% Triton-X100 and counterstained with DAPI. Anti-Pax7 antibody(+) or tdTomato(+) MuSCs per single muscle fiber were counted manually.

RNAscope

RNAscope for *Flt1* transcripts was performed as previously described (***Kann and Krauss, 2019***) on single muscle fibers from $Pax7^{tdT}$ mice using the RNAscope Probe - Mm-Flt1 (C1) (415541, ACDBio). Briefly, isolated EDL fibers are fixed in 4% PFA, washed with PBS, and dehydrated in 100% methanol. Subsequently, fibers are rehydrated in a stepwise gradient of decreasing methanol concentrations in PBS/0.1% Tween-20. Fibers are treated with a proteinase for 10 min, followed by hybridization, amplification, and fluorophore conjugation steps.

Histology and immunostaining for sections

The mouse tibialis anterior (TA) muscle was used for all histological analysis. Tissues were frozen fresh using LiN_2 chilled isopentane and stored at –80 °C. Eight µm thick transverse cryosections were used for all histological analysis. Hematoxylin & Eosin (HE) staining were performed as previously described (***Verma et al., 2010***). Sirius red (Direct Red 80, 365548, MilliporeSigma) staining was performed for muscle sections for fibrosis as previously described (***Shimizu-Motohashi et al., 2015***). Muscle sections were stained in Oil Red O solution (O1391-250ML, MilliporeSigma) as previously described (***Wang et al., 2017***). Anti-eMHC (F1.652, Developmental Study Hybridoma Bank) and anti-Laminin (L0663, MilliporeSigma) antibodies followed by anti-mouse Alexa-488 (A11001, ThermoFisher Scientific) and anti-rat Alexa-568 antibodies (A11077, ThermoFisher Scientific) were used for detection of regenerating muscle fibers. For capillary density measurement, anti-CD31 antibody (550274, BD Biosciences) was used for TA muscle sections followed by anti-rat Alexa-488 (A11006, ThermoFisher Scientific). Microscopic images were captured by a DP-1 digital camera attached to BX51 fluorescence microscope with 10×, 20×or 40×UPlanFLN objectives with cellSens Entry 1.11 (all from Olympus). Photoshop (Adobe) and Fiji (NIH) were used for image processing and manually enumerating the fiber feret's diameter (***Schindelin et al., 2012***).

Grip strength test

Forelimb grip strength test was performed following a previously published procedure (***Aartsma-Rus and van Putten, 2014***). Briefly, mice were gently pulled by the tail after fore limb-grasping a metal bar attached to a force transducer (Grip Strength Meter, 1027CSM-D52, Columbus Instruments). Grip strength tests were performed by the same blinded examiner. Five consecutive grip strength tests were recorded, and then mice were returned to the cage for a resting period of 20 min. Then, three series of pulls were performed each followed by 20 min resting period. The average of the three highest values out of the 15 values collected was normalized to the body weight for comparison.

Muscle perfusion

RBC flux was evaluated using the moorLabTM laser Doppler flow meter as previously described (***Verma et al., 2010***) with the MP7a probe that allows for collecting light from a deeper tissue level than standard probes according to the manufacturer's instructions (Moor Instruments). The fur from the right hind leg was removed using a chemical depilatory. Readings were taken using the probe

from at least 10 different spots on the TA muscle. The AU was determined as the average AU value during a plateau phase of each measurement.

RNA and genomic DNA isolation and qPCR

Cultured cells were washed with ice cold PBS and lysed on the place with Trizol. RNA was isolated using the DirectZol RNA Microprep Kit (R2062, Zymo Research) with on-column DNase digestion followed by cDNA synthesis using the Transcriptor First Strand cDNA synthesis kit (04379012001, Roche Molecular Diagnostics) using random primers. Genomic DNA for genotyping was isolated from mouse tail snips with lysis buffer containing Proteinase K (P2308, MilliporeSigma). qPCR was performed using GoTaq qPCR Master Mix (A6002, Promega). The input RNA amount was normalized across all samples and *18 S rRNA* or *HtatsF1* was used for normalization of qPCR across samples. Primer sequences are listed in Key Resources Table. All primers were synthesized as custom DNA oligos from Integrated DNA technologies (IDT).

Single-cell RNA sequencing and analysis

Cells for single-cell RNA-seq (scRNA-seq) were obtained from hind limb muscles of 2–3 month-old *Pax7^{tdT}:Flk1^{GFP}* mice following enzymatic digestion as previously described (***Liu et al., 2015***). Dead cells were excluded from the analysis using ZombieNIR (423105, Biolegends). TdTomato(+) and GFP(+) cells were sorted individually and then 20% of GFP(+) cells were spiked into 80% tdTomato(+). We loaded ~5000 cells into 1 channel of the Chromium system for each of these samples and prepared libraries according to the manufacturer's protocol using version 2.0 chemistry (10 x Genomics). Following capture and lysis, we synthesized cDNA and amplified for 12 cycles as per the manufacturer's protocol (10 X Genomics). The amplified cDNA was used to construct Illumina sequencing libraries that were each sequenced with ~300 K read/cell on one lane of an Illumina HiSeq 2500 machine. We used Cell Ranger 3.1 (10X Genomics) to process raw sequencing data. For A custom genome was constructed to include *eGFP-SV40*, *tdTomato-WPRE-BGHPolyA* and *Pax7-IRES-CreERT2* transgenes. Detailed step-by-step instructions can be found at https://github.com/verma014/10XCustomRef, (copy archived at ***Verma, 2020***). We carried out analyses of the filtered data using Seurat suite version 3.0 ***Stuart et al., 2019*** in ***RStudio Team, 2020***. For cell imputation, we utilized ALRA through the Seurat wrapper with default settings (***Linderman et al., 2022***). Additional scRNA-seq datasets were obtained from GEO and analyzed using the same method as listed above. A myogenic score was calculated based on the expression of *Myog*, *Pax7*, *Myod1*, and *Myf5*. Step-by-step instructions for the analysis can be found on https://github.com/verma014/10XCustomRef, (copy archived at ***Verma, 2020***).

Background subtraction

10 x Genomics scRNA-seq platform uses many more droplets than cells and so following a run, there are many droplets that do not have cells. These droplets still get sequenced with some of the RNA that is in the solution. This floating RNA can be used to estimate the 'background' in each droplet. A better description of this can be found by the developers of 'SoupX' (***Young and Behjati, 2020***). Since *Cdh5* expression has previously been verified in MuSCs using RNAscope, we were able to use it as a positive control to remove the background or 'soup' from our data. If *Cdh5* is absent from MuSC, we know that the background subtraction was too aggressive and that subtracting the Soup is not reliable in our case. In addition, we know certain genes that are considered to be specific for MuSCs, muscle ECs or muscle fibers based on the bulk RNA-seq (***Verma et al., 2018***). The top 5 genes that are specific to these population (and also detected by 10 x) were selected and used to show the background in our data set was 14.40% and 13.89% for the D0 and D3 dataset, respectively. The step-by-step instructions can be found on https://github.com/verma014/10XCustomRef, (copy archived at ***Verma, 2020***).

Bulk RNA-seq and microarray analysis

FASTQ files were downloaded from SRA using SRA-toolkit. Sequences were trimmed using trimmomatic to remove adapter contamination and low-quality reads. Trimmed sequences were mapped to mouse mm10 using Hisat2 (***Pertea et al., 2016***). Transcript assembly was performed using StringTie (***Pertea et al., 2016***). Cell type specificity was determined as previously described (***Verma et al.,***

2018). Microarray analysis was performed using the Affymetrix Transcriptome Analysis Console (TAC). Samples in each experiment were RNA normalized and the expression was acquired using the Affeymetrix Expression analysis console with gene level expression. Heatmaps were generated in Prism 9 (Graphpad, La Jolla, CA).

Quantification and statistical analysis

Statistical analysis was performed using Prism 9 (Graphpad, La Jolla, CA) or RStudio (***RStudio Team, 2020***). For comparison between two groups, an unpaired T-test was used. For comparison between multiple groups, a one-way ANOVA was used with multiple comparisons to the control. Distributions were compared using a chi-squared test. Graphing of the data was performed using Prism 9. Vector diagrams were modified using Graphic (Autodesk). All values are means ± SD unless noted otherwise. * indicates $p<0.05$, ** indicates $p<0.01$, *** indicates $p<0.001$.

Acknowledgements

We thank Minnesota Supercomputing Institute (MSI), University of Minnesota Imaging Center (UIC), University of Minnesota FACS Facility, and University of Minnesota Genomics Center (UMGC) for providing data for this paper. We also thank Jake Trask for critical reading of this paper. We thank Drs. Yosuke Mukouyama (National Institute of Health), Napoleone Ferrara (Genentech), Guo-Hua Fong (University of Connecticut) and Masatsugu Ema (Siga University of Medical Science) for providing *Vegfa*-$^{LoxP/LoxP}$, *Flt1*$^{LoxP/LoxP}$ and *Flk1-GFP* mice, respectively. This work was supported by NIHT32-GM008244 and NIHF30AR066454 to MV, NIAMS grant AR070231 to RSK, a fellowship of the Training Program in Stem Cell Research from the New York State Department of Health to A.P.K. (NYSTEM-C32561GG) and NIHR01AR062142, NIHR21AR070319, MDA Research Grant, and Regenerative Medicine Minnesota (RMM) Grant to AA.

Additional information

Funding

Funder	Grant reference number	Author
National Institutes of Health	NIHT32-GM008244	Mayank Verma
National Institutes of Health	NIHF30AR066454	Mayank Verma
National Institute of Arthritis and Musculoskeletal and Skin Diseases	AR070231	Robert S Krauss
New York State Stem Cell Science	NYSTEM-C32561GG	Allison P Kann
National Institute of Arthritis and Musculoskeletal and Skin Diseases	NIHR01AR062142	Atsushi Asakura
National Institute of Arthritis and Musculoskeletal and Skin Diseases	NIHR21AR070319	Atsushi Asakura
Muscular Dystrophy Association	MDA241600	Atsushi Asakura
Regenerative Medicine Minnesota	RMM 092319 TR 010	Atsushi Asakura

The funders had no role in study design, data collection and interpretation, or the decision to submit the work for publication.

Author contributions

Mayank Verma, Conceptualization, Data curation, Software, Formal analysis, Validation, Investigation, Visualization, Methodology, Writing - original draft, Writing - review and editing; Yoko Asakura, Xuerui Wang, Kasey Zhou, Mahmut Ünverdi, Allison P Kann, Data curation, Formal analysis; Robert S Krauss, Data curation, Formal analysis, Funding acquisition, Methodology, Writing - review and editing; Atsushi Asakura, Conceptualization, Resources, Data curation, Formal analysis, Supervision, Funding acquisition, Validation, Investigation, Visualization, Methodology, Writing - original draft, Project administration, Writing - review and editing

Author ORCIDs

Mayank Verma http://orcid.org/0000-0003-0167-0842
Yoko Asakura https://orcid.org/0000-0003-4107-4236
Allison P Kann http://orcid.org/0000-0003-0111-9081
Robert S Krauss http://orcid.org/0000-0002-7661-3335
Atsushi Asakura http://orcid.org/0000-0001-8078-1027

Ethics

The animals were housed in an SPF environment and were monitored by the Research Animal Resources (RAR) of the University of Minnesota. All protocols (2204-39969A) were approved by the Institutional Animal Care and Usage Committee (IACUC) of the University of Minnesota and complied with the NIH guidelines for the use of animals in research.

Decision letter and Author response

Decision letter https://doi.org/10.7554/eLife.73592.sa1
Author response https://doi.org/10.7554/eLife.73592.sa2

Additional files

Supplementary files

- Transparent reporting form
- Supplementary file 1. Gene Expression Omnibus (GEO) used for this paper was shown in this table, including their repositories and references.

Data availability

All the data was obtained from NCBI GEO. Microarrays of mouse MuSCs were obtained from GSE3483 (***Fukada et al., 2007***). scRNA-seq of MuSCs and muscle ECs was performed in this study (GSE129057). scRNA-seq of whole muscle was obtained from GSE143437 (***De Micheli et al., 2020***). Bulk RNA-seq of MuSCs, ECs and single muscle fibers was obtained from GSE108739 (***Verma et al., 2018***) and GSE64379 (***Ryall et al., 2015***). Bulk RNA-seq of TU-tagged RNA of MuSCs was obtained from GSE97399 (***van Velthoven et al., 2017***). Bulk RNA-seq of fixed and unfixed MuSCs was obtained from GSE113631 (***Yue et al., 2020***). Exercise, ALS, DMD, BMD, FSHD GSE3307, Early DMD GSE465, mdx GSE466, GRMD GSE69040, MuSCs GSE15155. All arrays were normalized to their respective controls. All arrays and RNA-seq data are listed in ***Supplementary file 1.***

The following dataset was generated:

Author(s)	Year	Dataset title	Dataset URL	Database and Identifier
Verma M, Asakura A	2020	Single-cell skeletal muscle satellite cells and endothelial cells during homeostasis and regeneration	https://www.ncbi.nlm.nih.gov/geo/query/acc.cgi?acc=GSE129057	NCBI Gene Expression Omnibus, GSE129057

The following previously published datasets were used:

Author(s)	Year	Dataset title	Dataset URL	Database and Identifier
Cosgrove BD, De Micheli AJ	2020	Single-cell transcriptomic atlas of the mouse regenerating muscle tissue	https://www.ncbi.nlm.nih.gov/geo/query/acc.cgi?acc=GSE143437	NCBI Gene Expression Omnibus, GSE143437
Verma M, Asakura A	2018	Skeletal muscle satellite cells, endothelial cells and single muscle fibers	https://www.ncbi.nlm.nih.gov/geo/query/acc.cgi?acc=GSE108739	NCBI Gene Expression Omnibus, GSE108739
Ryall JG, Dell'Orso S, Derfoul A, Juan A, Zare H, Feng X, Clermont D, Koulnis M, Gutierrez-Cruz G, Fulco M, Sartorelli V	2015	The NAD+-Dependent SIRT1 Deacetylase Translates a Metabolic Switch into Regulatory Epigenetics in Skeletal Muscle Stem Cells	https://www.ncbi.nlm.nih.gov/geo/query/acc.cgi?acc=GSE64379	NCBI Gene Expression Omnibus, GSE64379
Rando TA, van Velthoven CT	2017	Transcriptional profiling of quiescent muscle stem cells in vivo	https://www.ncbi.nlm.nih.gov/geo/query/acc.cgi?acc=GSE97399	NCBI Gene Expression Omnibus, GSE97399
Yue L, Wan R, Cheung TH	2020	Transcriptome profiling of quiescent muscle stem cells in vivo	https://www.ncbi.nlm.nih.gov/geo/query/acc.cgi?acc=GSE113631	NCBI Gene Expression Omnibus, GSE113631
Fukada S	2007	Genome-wide expression analysis of satellite cells	https://www.ncbi.nlm.nih.gov/geo/query/acc.cgi?acc=GSE3483	NCBI Gene Expression Omnibus, GSE3483
Hoffman EP	2005	Comparative profiling in 13 muscle disease groups	https://www.ncbi.nlm.nih.gov/geo/query/acc.cgi?acc=GSE3307	NCBI Gene Expression Omnibus, GSE3307
Chen YW, Zhao P, Borup R, Hoffman EP	2003	Expression profiling in the muscular dystrophies	https://www.ncbi.nlm.nih.gov/geo/query/acc.cgi?acc=GSE465	NCBI Gene Expression Omnibus, GSE465
Tseng BS, Zhao P, Pattison JS, Gordon SE, Granchelli JA, Madsen RW, Folk LC, Hoffman EP, Booth FW	2003	mRNA expression in regenerated mdx mouse skeletal muscle	https://www.ncbi.nlm.nih.gov/geo/query/acc.cgi?acc=GSE466	NCBI Gene Expression Omnibus, GSE466
Moreira YB, Vieira N	2015	Duchene Muscular Dystrophy Dogs Escapers and Affected Muscle Dogs Compared to Normal Dogs	https://www.ncbi.nlm.nih.gov/geo/query/acc.cgi?acc=GSE69040	NCBI Gene Expression Omnibus, GSE69040
Pallafacchina G, Montarras D, Regnault B, Buckingham M	2010	Gene profiling of quiescent and activated skeletal muscle satellite cells by an in vivo approach	https://www.ncbi.nlm.nih.gov/geo/query/acc.cgi?acc=GSE15155	NCBI Gene Expression Omnibus, GSE15155

References

Aartsma-Rus A, van Putten M. 2014. Assessing functional performance in the mdx mouse model. *Journal of Visualized Experiments* **01**:51303. DOI: https://doi.org/10.3791/51303, PMID: 24747372

Arsic N, Zacchigna S, Zentilin L, Ramirez-Correa G, Pattarini L, Salvi A, Sinagra G, Giacca M. 2004. Vascular endothelial growth factor stimulates skeletal muscle regeneration in vivo. *Molecular Therapy* **10**:844–854. DOI: https://doi.org/10.1016/j.ymthe.2004.08.007, PMID: 15509502

Asakura A, Komaki M, Rudnicki M. 2001. Muscle satellite cells are multipotential stem cells that exhibit myogenic, osteogenic, and adipogenic differentiation. *Differentiation; Research in Biological Diversity* **68**:245–253. DOI: https://doi.org/10.1046/j.1432-0436.2001.680412.x, PMID: 11776477

Asakura A, Seale P, Girgis-Gabardo A, Rudnicki MA. 2002. Myogenic specification of side population cells in skeletal muscle. *The Journal of Cell Biology* **159**:123–134. DOI: https://doi.org/10.1083/jcb.200202092, PMID: 12379804

Bae DG, Kim TD, Li G, Yoon WH, Chae CB. 2005. Anti-flt1 peptide, a vascular endothelial growth factor receptor 1-specific hexapeptide, inhibits tumor growth and metastasis. *Clinical Cancer Research* **11**:2651–2661. DOI: https://doi.org/10.1158/1078-0432.CCR-04-1564, PMID: 15814646

Bakay M, Wang Z, Melcon G, Schiltz L, Xuan J, Zhao P, Sartorelli V, Seo J, Pegoraro E, Angelini C, Shneiderman B, Escolar D, Chen YW, Winokur ST, Pachman LM, Fan C, Mandler R, Nevo Y, Gordon E, Zhu Y, et al. 2006. Nuclear envelope dystrophies show a transcriptional fingerprint suggesting disruption of Rb-MyoD pathways in muscle regeneration. *Brain* **129**:996–1013. DOI: https://doi.org/10.1093/brain/awl023, PMID: 16478798

Boldrin L, Zammit PS, Morgan JE. 2015. Satellite cells from dystrophic muscle retain regenerative capacity. *Stem Cell Research* **14**:20–29. DOI: https://doi.org/10.1016/j.scr.2014.10.007, PMID: 25460248

Bosco J, Zhou Z, Gabriëls S, Verma M, Liu N, Miller BK, Gu S, Lundberg DM, Huang Y, Brown E, Josiah S, Meiyappan M, Traylor MJ, Chen N, Asakura A, De Jonge N, Blanchetot C, de Haard H, Duffy HS, Keefe D. 2021. VEGFR-1/Flt-1 inhibition increases angiogenesis and improves muscle function in a mouse model of Duchenne muscular dystrophy. *Molecular Therapy. Methods & Clinical Development* **21**:369–381. DOI: https://doi.org/10.1016/j.omtm.2021.03.013, PMID: 33898634

Bouchentouf M, Benabdallah BF, Bigey P, Yau TM, Scherman D, Tremblay JP. 2008. Vascular endothelial growth factor reduced hypoxia-induced death of human myoblasts and improved their engraftment in mouse muscles. *Gene Therapy* **15**:404–414. DOI: https://doi.org/10.1038/sj.gt.3303059, PMID: 18079754

Bryan BA, Walshe TE, Mitchell DC, Havumaki JS, Saint-Geniez M, Maharaj AS, Maldonado AE, D'Amore PA. 2008. Coordinated vascular endothelial growth factor expression and signaling during skeletal myogenic differentiation. *Molecular Biology of the Cell* **19**:994–1006. DOI: https://doi.org/10.1091/mbc.e07-09-0856, PMID: 18094043

Chapman VM, Miller DR, Armstrong D, Caskey CT. 1989. Recovery of induced mutations for X chromosome-linked muscular dystrophy in mice. *PNAS* **86**:1292–1296. DOI: https://doi.org/10.1073/pnas.86.4.1292, PMID: 2919177

Charville GW, Cheung TH, Yoo B, Santos PJ, Lee GK, Shrager JB, Rando TA. 2015. Ex vivo expansion and in vivo self-renewal of human muscle stem cells. *Stem Cell Reports* **5**:621–632. DOI: https://doi.org/10.1016/j.stemcr.2015.08.004, PMID: 26344908

Chen YW, Zhao P, Borup R, Hoffman EP. 2000. Expression profiling in the muscular dystrophies: identification of novel aspects of molecular pathophysiology. *The Journal of Cell Biology* **151**:1321–1336. DOI: https://doi.org/10.1083/jcb.151.6.1321, PMID: 11121445

Chen W, Wang YX, Ritso M, Perkins TJ, Rudnicki MA. 2022. KDR Signaling in Muscle Stem Cells Promotes Asymmetric Division and Progenitor Generation for Efficient Regeneration. *bioRxiv*. DOI: https://doi.org/10.1101/2022.06.27.497734

Chestnut B, Casie Chetty S, Koenig AL, Sumanas S. 2020. Single-cell transcriptomic analysis identifies the conversion of zebrafish Etv2-deficient vascular progenitors into skeletal muscle. *Nature Communications* **11**:2796. DOI: https://doi.org/10.1038/s41467-020-16515-y, PMID: 32493965

Christov C, Chrétien F, Abou-Khalil R, Bassez G, Vallet G, Authier F-J, Bassaglia Y, Shinin V, Tajbakhsh S, Chazaud B, Gherardi RK. 2007. Muscle satellite cells and endothelial cells: close neighbors and privileged partners. *Molecular Biology of the Cell* **18**:1397–1409. DOI: https://doi.org/10.1091/mbc.e06-08-0693, PMID: 17287398

De Angelis L, Berghella L, Coletta M, Lattanzi L, Zanchi M, Cusella-De Angelis MG, Ponzetto C, Cossu G. 1999. Skeletal myogenic progenitors originating from embryonic dorsal aorta coexpress endothelial and myogenic markers and contribute to postnatal muscle growth and regeneration. *The Journal of Cell Biology* **147**:869–878. DOI: https://doi.org/10.1083/jcb.147.4.869, PMID: 10562287

Delavar H, Nogueira L, Wagner PD, Hogan MC, Metzger D, Breen EC. 2014. Skeletal myofiber VEGF is essential for the exercise training response in adult mice. *American Journal of Physiology-Regulatory, Integrative and Comparative Physiology* **306**:R586–R595. DOI: https://doi.org/10.1152/ajpregu.00522.2013

De Micheli AJ, Laurilliard EJ, Heinke CL, Ravichandran H, Fraczek P, Soueid-Baumgarten S, De Vlaminck I, Elemento O, Cosgrove BD. 2020. Single-cell analysis of the muscle stem cell hierarchy identifies heterotypic communication signals involved in skeletal muscle regeneration. *Cell Reports* **30**:3583–3595. DOI: https://doi.org/10.1016/j.celrep.2020.02.067, PMID: 32160558

Desrochers LM, Antonyak MA, Cerione RA. 2016. Extracellular vesicles: Satellites of information transfer in cancer and stem cell biology. *Developmental Cell* **37**:301–309. DOI: https://doi.org/10.1016/j.devcel.2016.04.019, PMID: 27219060

Domigan CK, Warren CM, Antanesian V, Happel K, Ziyad S, Lee S, Krall A, Duan L, Torres-Collado AX, Castellani LW, Elashoff D, Christofk HR, van der Bliek AM, Potente M, Iruela-Arispe ML. 2015. Autocrine VEGF maintains endothelial survival through regulation of metabolism and autophagy. *Journal of Cell Science* **128**:2236–2248. DOI: https://doi.org/10.1242/jcs.163774, PMID: 25956888

Drummond CJ, Hatley ME. 2018. A Case of mistaken identity: Rhabdomyosarcoma development from endothelial progenitor cells. *Molecular & Cellular Oncology* **5**:e1448246. DOI: https://doi.org/10.1080/23723556.2018.1448246, PMID: 30250910

Eichmann A, Marcelle C, Bréant C, Le Douarin NM. 1993. Two molecules related to the VEGF receptor are expressed in early endothelial cells during avian embryonic development. *Mechanisms of Development* **42**:33–48. DOI: https://doi.org/10.1016/0925-4773(93)90096-g, PMID: 8396413

Ema M, Takahashi S, Rossant J. 2006. Deletion of the selection cassette, but not cis-acting elements, in targeted Flk1-lacZ allele reveals Flk1 expression in multipotent mesodermal progenitors. *Blood* **107**:111–117. DOI: https://doi.org/10.1182/blood-2005-05-1970, PMID: 16166582

Esner M, Meilhac SM, Relaix F, Nicolas JF, Cossu G, Buckingham ME. 2006. Smooth muscle of the dorsal aorta shares a common clonal origin with skeletal muscle of the myotome. *Development* **133**:737–749. DOI: https://doi.org/10.1242/dev.02226, PMID: 16436625

Fukada S, Uezumi A, Ikemoto M, Masuda S, Segawa M, Tanimura N, Yamamoto H, Miyagoe-Suzuki Y, Takeda S. 2007. Molecular signature of quiescent satellite cells in adult skeletal muscle. *Stem Cells* **25**:2448–2459. DOI: https://doi.org/10.1634/stemcells.2007-0019, PMID: 17600112

Gay L, Miller MR, Ventura PB, Devasthali V, Vue Z, Thompson HL, Temple S, Zong H, Cleary MD, Stankunas K, Doe CQ. 2013. Mouse TU tagging: a chemical/genetic intersectional method for purifying cell type-specific nascent RNA. *Genes & Development* **27**:98–115. DOI: https://doi.org/10.1101/gad.205278.112, PMID: 23307870

Gerber HP, McMurtrey A, Kowalski J, Yan M, Keyt BA, Dixit V, Ferrara N. 1998. Vascular endothelial growth factor regulates endothelial cell survival through the phosphatidylinositol 3'-kinase/Akt signal transduction pathway. Requirement for Flk-1/KDR activation. *The Journal of Biological Chemistry* **273**:30336–30343. DOI: https://doi.org/10.1074/jbc.273.46.30336, PMID: 9804796

Gerber HP, Hillan KJ, Ryan AM, Kowalski J, Keller GA, Rangell L, Wright BD, Radtke F, Aguet M, Ferrara N. 1999. VEGF is required for growth and survival in neonatal mice. *Development* **126**:1149–1159. DOI: https://doi.org/10.1242/dev.126.6.1149, PMID: 10021335

Germani A, Di Carlo A, Mangoni A, Straino S, Giacinti C, Turrini P, Biglioli P, Capogrossi MC. 2003. Vascular endothelial growth factor modulates skeletal myoblast function. *The American Journal of Pathology* **163**:1417–1428. DOI: https://doi.org/10.1016/S0002-9440(10)63499-2, PMID: 14507649

Giordani L, He GJ, Negroni E, Sakai H, Law JYC, Siu MM, Wan R, Corneau A, Tajbakhsh S, Cheung TH, Le Grand F. 2019. High-dimensional single-cell cartography reveals novel skeletal muscle-resident cell populations. *Molecular Cell* **74**:609–621. DOI: https://doi.org/10.1016/j.molcel.2019.02.026, PMID: 30922843

Goel AJ, Rieder MK, Arnold HH, Radice GL, Krauss RS. 2017. Niche cadherins control the quiescence-to-activation transition in muscle stem cells. *Cell Reports* **21**:2236–2250. DOI: https://doi.org/10.1016/j.celrep.2017.10.102, PMID: 29166613

Groppa E, Martini P, Derakhshan N, Theret M, Ritso M, Tung LW, Wang YX, Soliman H, Hamer MS, Stankiewicz L, Eisner C, Erwan LN, Chang C, Yi L, Yuan JH, Kong S, Weng C, Adams J, Chang L, Peng A, et al. 2023. Spatial compartmentalization of signaling imparts source-specific functions on secreted factors. *Cell Reports* **42**:112051. DOI: https://doi.org/10.1016/j.celrep.2023.112051, PMID: 36729831

Hardy D, Besnard A, Latil M, Jouvion G, Briand D, Thépenier C, Pascal Q, Guguin A, Gayraud-Morel B, Cavaillon JM, Tajbakhsh S, Rocheteau P, Chrétien F. 2016. Comparative study of injury models for studying muscle regeneration in mice. *PLOS ONE* **11**:e0147198. DOI: https://doi.org/10.1371/journal.pone.0147198, PMID: 26807982

Hirai H, Verma M, Watanabe S, Tastad C, Asakura Y, Asakura A. 2010. MyoD regulates apoptosis of myoblasts through microRNA-mediated down-regulation of Pax3. *The Journal of Cell Biology* **191**:347–365. DOI: https://doi.org/10.1083/jcb.201006025, PMID: 20956382

Ho VC, Duan LJ, Cronin C, Liang BT, Fong GH. 2012. Elevated vascular endothelial growth factor receptor-2 abundance contributes to increased angiogenesis in vascular endothelial growth factor receptor-1-deficient mice. *Circulation* **126**:741–752. DOI: https://doi.org/10.1161/CIRCULATIONAHA.112.091603, PMID: 22753193

Huang P, Schulz TJ, Beauvais A, Tseng YH, Gussoni E. 2014. Intramuscular adipogenesis is inhibited by myo-endothelial progenitors with functioning Bmpr1a signalling. *Nature Communications* **5**:4063. DOI: https://doi.org/10.1038/ncomms5063, PMID: 24898859

Hutcheson DA, Kardon G. 2009. Genetic manipulations reveal dynamic cell and gene functions: Cre-ating a new view of myogenesis. *Cell Cycle* **8**:3675–3678. DOI: https://doi.org/10.4161/cc.8.22.9992, PMID: 19844163

Kann AP, Krauss RS. 2019. Multiplexed RNAscope and immunofluorescence on whole-mount skeletal myofibers and their associated stem cells. *Development* **146**:dev179259. DOI: https://doi.org/10.1242/dev.179259, PMID: 31519691

Kardon G, Campbell JK, Tabin CJ. 2002. Local extrinsic signals determine muscle and endothelial cell fate and patterning in the vertebrate limb. *Developmental Cell* **3**:533–545. DOI: https://doi.org/10.1016/s1534-5807(02)00291-5, PMID: 12408805

Keifer OP Jr, O'Connor DM, Boulis NM. 2014. Gene and protein therapies utilizing VEGF for ALS. *Pharmacology & Therapeutics* **141**:261–271. DOI: https://doi.org/10.1016/j.pharmthera.2013.10.009, PMID: 24177067

Kobayashi H, Butler JM, O'Donnell R, Kobayashi M, Ding B-S, Bonner B, Chiu VK, Nolan DJ, Shido K, Benjamin L, Rafii S. 2010. Angiocrine factors from Akt-activated endothelial cells balance self-renewal and differentiation of haematopoietic stem cells. *Nature Cell Biology* **12**:1046–1056. DOI: https://doi.org/10.1038/ncb2108, PMID: 20972423

Kodippili K, Thorne PK, Laughlin MH, Duan D. 2021. Dystrophin deficiency impairs vascular structure and function in the canine model of Duchenne muscular dystrophy. *The Journal of Pathology* **254**:589–605. DOI: https://doi.org/10.1002/path.5704, PMID: 33999411

Lagha M, Brunelli S, Messina G, Cumano A, Kume T, Relaix F, Buckingham ME. 2009. Pax3:Foxc2 reciprocal repression in the somite modulates muscular versus vascular cell fate choice in multipotent progenitors. *Developmental Cell* **17**:892–899. DOI: https://doi.org/10.1016/j.devcel.2009.10.021, PMID: 20059958

Latroche C, Matot B, Martins-Bach A, Briand D, Chazaud B, Wary C, Carlier PG, Chrétien F, Jouvion G. 2015. Structural and functional alterations of skeletal muscle microvasculature in dystrophin-deficient mdx mice. *The American Journal of Pathology* **185**:2482–2494. DOI: https://doi.org/10.1016/j.ajpath.2015.05.009, PMID: 26193666

Latroche C, Weiss-Gayet M, Muller L, Gitiaux C, Leblanc P, Liot S, Ben-Larbi S, Abou-Khalil R, Verger N, Bardot P, Magnan M, Chrétien F, Mounier R, Germain S, Chazaud B. 2017. Coupling between myogenesis and angiogenesis during skeletal muscle regeneration is stimulated by restorative macrophages. *Stem Cell Reports* **9**:2018–2033. DOI: https://doi.org/10.1016/j.stemcr.2017.10.027, PMID: 29198825

Le Grand F, Auda-Boucher G, Levitsky D, Rouaud T, Fontaine-Pérus J, Gardahaut MF. 2004. Endothelial cells within embryonic skeletal muscles: a potential source of myogenic progenitors. *Experimental Cell Research* **301**:232–241. DOI: https://doi.org/10.1016/j.yexcr.2004.07.028, PMID: 15530859

Lee S, Chen TT, Barber CL, Jordan MC, Murdock J, Desai S, Ferrara N, Nagy A, Roos KP, Iruela-Arispe ML. 2007. Autocrine VEGF signaling is required for vascular homeostasis. *Cell* **130**:691–703. DOI: https://doi.org/10.1016/j.cell.2007.06.054, PMID: 17719546

Li Y, Zhang F, Nagai N, Tang Z, Zhang S, Scotney P, Lennartsson J, Zhu C, Qu Y, Fang C, Hua J, Matsuo O, Fong GH, Ding H, Cao Y, Becker KG, Nash A, Heldin CH, Li X. 2008. VEGF-B inhibits apoptosis via VEGFR-1-mediated suppression of the expression of BH3-only protein genes in mice and rats. *The Journal of Clinical Investigation* **118**:913–923. DOI: https://doi.org/10.1172/JCI33673, PMID: 18259607

Linderman GC, Zhao J, Roulis M, Bielecki P, Flavell RA, Nadler B, Kluger Y. 2022. Zero-preserving imputation of single-cell RNA-seq data. *Nature Communications* **13**:192. DOI: https://doi.org/10.1038/s41467-021-27729-z, PMID: 35017482

Liu Y, Berendsen AD, Jia S, Lotinun S, Baron R, Ferrara N, Olsen BR. 2012. Intracellular VEGF regulates the balance between osteoblast and adipocyte differentiation. *Journal of Clinical Investigation* **122**:3101–3113. DOI: https://doi.org/10.1172/JCI61209

Liu L, Cheung TH, Charville GW, Rando TA. 2015. Isolation of skeletal muscle stem cells by fluorescence-activated cell sorting. *Nature Protocols* **10**:1612–1624. DOI: https://doi.org/10.1038/nprot.2015.110

Loiben AM, Soueid-Baumgarten S, Kopyto RF, Bhattacharya D, Kim JC, Cosgrove BD. 2017. Data-modeling identifies conflicting signaling axes governing myoblast proliferation and differentiation responses to diverse ligand stimuli. *Cellular and Molecular Bioengineering* **10**:433–450. DOI: https://doi.org/10.1007/s12195-017-0508-5, PMID: 31719871

Mac Gabhann F, Qutub AA, Annex BH, Popel AS. 2010. Systems biology of pro-angiogenic therapies targeting the VEGF system. *Wiley Interdisciplinary Reviews. Systems Biology and Medicine* **2**:694–707. DOI: https://doi.org/10.1002/wsbm.92, PMID: 20890966

Madisen L, Zwingman TA, Sunkin SM, Oh SW, Zariwala HA, Gu H, Ng LL, Palmiter RD, Hawrylycz MJ, Jones AR, Lein ES, Zeng H. 2010. A robust and high-throughput Cre reporting and characterization system for the whole mouse brain. *Nature Neuroscience* **13**:133–140. DOI: https://doi.org/10.1038/nn.2467, PMID: 20023653

Mayeuf-Louchart A, Lagha M, Danckaert A, Rocancourt D, Relaix F, Vincent SD, Buckingham M. 2014. Notch regulation of myogenic versus endothelial fates of cells that migrate from the somite to the limb. *PNAS* **111**:8844–8849. DOI: https://doi.org/10.1073/pnas.1407606111, PMID: 24927569

Mayeuf-Louchart A, Montarras D, Bodin C, Kume T, Vincent SD, Buckingham M. 2016. Endothelial cell specification in the somite is compromised in Pax3-positive progenitors of Foxc1/2 conditional mutants, with loss of forelimb myogenesis. *Development* **143**:872–879. DOI: https://doi.org/10.1242/dev.128017, PMID: 26839363

Mercatelli N, Dimauro I, Ciafré SA, Farace MG, Caporossi D. 2010. AlphaB-crystallin is involved in oxidative stress protection determined by VEGF in skeletal myoblasts. *Free Radical Biology & Medicine* **49**:374–382. DOI: https://doi.org/10.1016/j.freeradbiomed.2010.04.027, PMID: 20441791

Messina S, Mazzeo A, Bitto A, Aguennouz M, Migliorato A, De Pasquale MG, Minutoli L, Altavilla D, Zentilin L, Giacca M, Squadrito F, Vita G. 2007. VEGF overexpression via adeno-associated virus gene transfer promotes skeletal muscle regeneration and enhances muscle function in mdx mice. *FASEB Journal* **21**:3737–3746. DOI: https://doi.org/10.1096/fj.07-8459com, PMID: 17575261

Minasi MG, Riminucci M, De Angelis L, Borello U, Berarducci B, Innocenzi A, Caprioli A, Sirabella D, Baiocchi M, De Maria R, Boratto R, Jaffredo T, Broccoli V, Bianco P, Cossu G. 2002. The meso-angioblast: a multipotent, self-renewing cell that originates from the dorsal aorta and differentiates into most mesodermal tissues. *Development* **129**:2773–2783. DOI: https://doi.org/10.1242/dev.129.11.2773, PMID: 12015303

Miquerol L, Gertsenstein M, Harpal K, Rossant J, Nagy A. 1999. Multiple developmental roles of VEGF suggested by a LacZ-tagged allele. *Developmental Biology* **212**:307–322. DOI: https://doi.org/10.1006/dbio.1999.9355, PMID: 10433823

Motohashi N, Asakura A. 2014. Muscle satellite cell heterogeneity and self-renewal. *Frontiers in Cell and Developmental Biology* **2**:1. DOI: https://doi.org/10.3389/fcell.2014.00001, PMID: 25364710

Motohashi N, Asakura Y, Asakura A. 2014. Isolation, culture, and transplantation of muscle satellite cells. *Journal of Visualized Experiments* **50846**:50846. DOI: https://doi.org/10.3791/50846, PMID: 24747722

Motoike T, Markham DW, Rossant J, Sato TN. 2003. Evidence for novel fate of Flk1+ progenitor: contribution to muscle lineage. *Genesis* **35**:153–159. DOI: https://doi.org/10.1002/gene.10175, PMID: 12640619

Murach KA, Vechetti IJ, Van Pelt DW, Crow SE, Dungan CM, Figueiredo VC, Kosmac K, Fu X, Richards CI, Fry CS, McCarthy JJ, Peterson CA. 2020. Fusion-independent satellite cell communication to muscle fibers during load-induced hypertrophy. *Function* **1**:zqaa009. DOI: https://doi.org/10.1093/function/zqaa009, PMID: 32864621

Murphy MM, Lawson JA, Mathew SJ, Hutcheson DA, Kardon G. 2011. Satellite cells, connective tissue fibroblasts and their interactions are crucial for muscle regeneration. *Journal of Cell Science* **124**:e1. DOI: https://doi.org/10.1242/jcs098228

Noren DP, Chou WH, Lee SH, Qutub AA, Warmflash A, Wagner DS, Popel AS, Levchenko A. 2016. Endothelial cells decode VEGF-mediated Ca2+ signaling patterns to produce distinct functional responses. *Science Signaling* **9**:ra20. DOI: https://doi.org/10.1126/scisignal.aad3188, PMID: 26905425

Okabe K, Kobayashi S, Yamada T, Kurihara T, Tai-Nagara I, Miyamoto T, Mukouyama Y, Sato TN, Suda T, Ema M, Kubota Y. 2014. Neurons limit angiogenesis by titrating VEGF in retina. *Cell* **159**:584–596. DOI: https://doi.org/10.1016/j.cell.2014.09.025, PMID: 25417109

Olfert IM, Howlett RA, Tang K, Dalton ND, Gu Y, Peterson KL, Wagner PD, Breen EC. 2009. Muscle-specific VEGF deficiency greatly reduces exercise endurance in mice. *The Journal of Physiology* **587**:1755–1767. DOI: https://doi.org/10.1113/jphysiol.2008.164384, PMID: 19237429

Pallafacchina G, François S, Regnault B, Czarny B, Dive V, Cumano A, Montarras D, Buckingham M. 2010. An adult tissue-specific stem cell in its niche: a gene profiling analysis of in vivo quiescent and activated muscle satellite cells. *Stem Cell Research* **4**:77–91. DOI: https://doi.org/10.1016/j.scr.2009.10.003, PMID: 19962952

Pertea M, Kim D, Pertea GM, Leek JT, Salzberg SL. 2016. Transcript-level expression analysis of RNA-seq experiments with HISAT, StringTie and Ballgown. *Nature Protocols* **11**:1650–1667. DOI: https://doi.org/10.1038/nprot.2016.095, PMID: 27560171

Podkalicka P, Mucha O, Kaziród K, Bronisz-Budzyńska I, Ostrowska-Paton S, Tomczyk M, Andrysiak K, Stępniewski J, Dulak J, Łoboda A. 2021. Age-dependent dysregulation of muscle vasculature and blood flow recovery after hindlimb ischemia in the *mdx* model of duchenne muscular dystrophy. *Biomedicines* **9**:481. DOI: https://doi.org/10.3390/biomedicines9050481, PMID: 33925757

Poesen K, Lambrechts D, Van Damme P, Dhondt J, Bender F, Frank N, Bogaert E, Claes B, Heylen L, Verheyen A, Raes K, Tjwa M, Eriksson U, Shibuya M, Nuydens R, Van Den Bosch L, Meert T, D'Hooge R, Sendtner M, Robberecht W, et al. 2008. Novel role for vascular endothelial growth factor (VEGF) receptor-1 and its ligand VEGF-B in motor neuron degeneration. *The Journal of Neuroscience* **28**:10451–10459. DOI: https://doi.org/10.1523/JNEUROSCI.1092-08.2008, PMID: 18923022

Roobrouck VD, Clavel C, Jacobs SA, Ulloa-Montoya F, Crippa S, Sohni A, Roberts SJ, Luyten FP, Van Gool SW, Sampaolesi M, Delforge M, Luttun A, Verfaillie CM. 2011. Differentiation potential of human postnatal mesenchymal stem cells, mesoangioblasts, and multipotent adult progenitor cells reflected in their transcriptome and partially influenced by the culture conditions. *Stem Cells* **29**:871–882. DOI: https://doi.org/10.1002/stem.633, PMID: 21433224

RStudio Team. 2020. Rstudio: integrated development for R. Boston, MA. RStudio, PBC. http://www.rstudio.com/pod

Ryall JG, Dell'Orso S, Derfoul A, Juan A, Zare H, Feng X, Clermont D, Koulnis M, Gutierrez-Cruz G, Fulco M, Sartorelli V. 2015. The NAD(+)-dependent SIRT1 deacetylase translates a metabolic switch into regulatory epigenetics in skeletal muscle stem cells. *Cell Stem Cell* **16**:171–183. DOI: https://doi.org/10.1016/j.stem.2014.12.004, PMID: 25600643

Sakurai H, Okawa Y, Inami Y, Nishio N, Isobe K. 2008. Paraxial mesodermal progenitors derived from mouse embryonic stem cells contribute to muscle regeneration via differentiation into muscle satellite cells. *Stem Cells* **26**:1865–1873. DOI: https://doi.org/10.1634/stemcells.2008-0173, PMID: 18450822

Schindelin J, Arganda-Carreras I, Frise E, Kaynig V, Longair M, Pietzsch T, Preibisch S, Rueden C, Saalfeld S, Schmid B, Tinevez JY, White DJ, Hartenstein V, Eliceiri K, Tomancak P, Cardona A. 2012. Fiji: an open-source platform for biological-image analysis. *Nature Methods* **9**:676–682. DOI: https://doi.org/10.1038/nmeth.2019, PMID: 22743772

Shimizu-Motohashi Y, Asakura Y, Motohashi N, Belur NR, Baumrucker MG, Asakura A. 2015. Pregnancy-induced amelioration of muscular dystrophy phenotype in mdx mice via muscle membrane stabilization effect of glucocorticoid. *PLOS ONE* **10**:e0120325. DOI: https://doi.org/10.1371/journal.pone.0120325, PMID: 25775477

Stuart T, Butler A, Hoffman P, Hafemeister C, Papalexi E, Mauck WM, Hao Y, Stoeckius M, Smibert P, Satija R. 2019. Comprehensive integration of single-cell data. *Cell* **177**:1888–1902.. DOI: https://doi.org/10.1016/j.cell.2019.05.031, PMID: 31178118

Tamaki T, Akatsuka A, Ando K, Nakamura Y, Matsuzawa H, Hotta T, Roy RR, Edgerton VR. 2002. Identification of myogenic-endothelial progenitor cells in the interstitial spaces of skeletal muscle. *The Journal of Cell Biology* **157**:571–577. DOI: https://doi.org/10.1083/jcb.200112106, PMID: 11994315

Tang K, Breen EC, Gerber HP, Ferrara NMA, Wagner PD. 2004. Capillary regression in vascular endothelial growth factor-deficient skeletal muscle. *Physiological Genomics* **18**:63–69. DOI: https://doi.org/10.1152/physiolgenomics.00023.2004, PMID: 15084712

Torre E, Dueck H, Shaffer S, Gospocic J, Gupte R, Bonasio R, Kim J, Murray J, Raj A. 2018. Rare Cell Detection by Single-Cell RNA Sequencing as Guided by Single-Molecule RNA FISH. *Cell Systems* **6**:171–179.. DOI: https://doi.org/10.1016/j.cels.2018.01.014, PMID: 29454938

Tozer S, Bonnin M-A, Relaix F, Di Savino S, García-Villalba P, Coumailleau P, Duprez D. 2007. Involvement of vessels and PDGFB in muscle splitting during chick limb development. *Development* **134**:2579–2591. DOI: https://doi.org/10.1242/dev.02867, PMID: 17553906

Tseng BS, Zhao P, Pattison JS, Gordon SE, Granchelli JA, Madsen RW, Folk LC, Hoffman EP, Booth FW. 2002. Regenerated mdx mouse skeletal muscle shows differential mRNA expression. *Journal of Applied Physiology* **93**:537–545. DOI: https://doi.org/10.1152/japplphysiol.00202.2002, PMID: 12133862

Turaç G, Hindley CJ, Thomas R, Davis JA, Deleidi M, Gasser T, Karaöz E, Pruszak J. 2013. Combined flow cytometric analysis of surface and intracellular antigens reveals surface molecule markers of human neuropoiesis. *PLOS ONE* **8**:e68519. DOI: https://doi.org/10.1371/journal.pone.0068519, PMID: 23826393

van Velthoven CTJ, de Morree A, Egner IM, Brett JO, Rando TA. 2017. Transcriptional profiling of quiescent muscle stem cells invivo. *Cell Reports* **21**:1994–2004. DOI: https://doi.org/10.1016/j.celrep.2017.10.037, PMID: 29141228

Veldman MB, Zhao C, Gomez GA, Lindgren AG, Huang H, Yang H, Yao S, Martin BL, Kimelman D, Lin S. 2013. Transdifferentiation of fast skeletal muscle into functional endothelium in vivo by transcription factor Etv2. *PLOS Biology* **11**:e1001590. DOI: https://doi.org/10.1371/journal.pbio.1001590, PMID: 23853546

Vempati P, Popel AS, Mac Gabhann F. 2014. Extracellular regulation of VEGF: isoforms, proteolysis, and vascular patterning. *Cytokine & Growth Factor Reviews* **25**:1–19. DOI: https://doi.org/10.1016/j.cytogfr.2013.11.002, PMID: 24332926

Verma M, Asakura Y, Hirai H, Watanabe S, Tastad C, Fong GH, Ema M, Call JA, Lowe DA, Asakura A. 2010. Flt-1 haploinsufficiency ameliorates muscular dystrophy phenotype by developmentally increased vasculature in mdx mice. *Human Molecular Genetics* **19**:4145–4159. DOI: https://doi.org/10.1093/hmg/ddq334, PMID: 20705734

Verma M, Asakura Y, Murakonda BSR, Pengo T, Latroche C, Chazaud B, McLoon LK, Asakura A. 2018. Muscle Satellite Cell Cross-Talk with a Vascular Niche Maintains Quiescence via VEGF and Notch Signaling. *Cell Stem Cell* **23**:530–543. DOI: https://doi.org/10.1016/j.stem.2018.09.007, PMID: 30290177

Verma M, Shimizu-Motohashi Y, Asakura Y, Ennen JP, Bosco J, Zhou Z, Fong GH, Josiah S, Keefe D, Asakura A. 2019. Inhibition of FLT1 ameliorates muscular dystrophy phenotype by increased vasculature in a mouse model of Duchenne muscular dystrophy. *PLOS Genetics* **15**:e1008468. DOI: https://doi.org/10.1371/journal.pgen.1008468, PMID: 31877123

VermaM. 2020. 10Xcustomref. swh:1:rev:9a7cc8726686e1aed2d0fa5abd60a1a884463802. Software Heritage. https://archive.softwareheritage.org/swh:1:dir:6723983bc03da139f5a3ff1094de9f35210e5d14;origin=https://github.com/verma014/10XCustomRef;visit=swh:1:snp:09c554a8975d34263a1ba160f5f50645d8ce8fea;anchor=swh:1:rev:9a7cc8726686e1aed2d0fa5abd60a1a884463802

Vieira NM, Elvers I, Alexander MS, Moreira YB, Eran A, Gomes JP, Marshall JL, Karlsson EK, Verjovski-Almeida S, Lindblad-Toh K, Kunkel LM, Zatz M. 2015. Jagged 1 rescues the duchenne muscular dystrophy phenotype. *Cell* **163**:1204–1213. DOI: https://doi.org/10.1016/j.cell.2015.10.049, PMID: 26582133

Wagner PD, Olfert IM, Tang K, Breen EC. 2006. Muscle-targeted deletion of VEGF and exercise capacity in mice. *Respiratory Physiology & Neurobiology* **151**:159–166. DOI: https://doi.org/10.1016/j.resp.2005.09.007

Wang C, Liu W, Nie Y, Qaher M, Horton HE, Yue F, Asakura A, Kuang S. 2017. Loss of MyoD promotes fate transdifferentiation of myoblasts into brown adipocytes. *EBioMedicine* **16**:212–223. DOI: https://doi.org/10.1016/j.ebiom.2017.01.015

Xin C, Chu X, Wei W, Kuang B, Wang Y, Tang Y, Chen J, You H, Li C, Wang B. 2021. Combined gene therapy via VEGF and mini-dystrophin synergistically improves pathologies in temporalis muscle of dystrophin/utrophin double knockout mice. *Human Molecular Genetics* **30**:1349–1359. DOI: https://doi.org/10.1093/hmg/ddab120, PMID: 33987645

Yan H, Guo Y, Zhang P, Zu L, Dong X, Chen L, Tian J, Fan X, Wang N, Wu X, Gao W. 2005. Superior neovascularization and muscle regeneration in ischemic skeletal muscles following VEGF gene transfer by rAAV1 pseudotyped vectors. *Biochemical and Biophysical Research Communications* **336**:287–298. DOI: https://doi.org/10.1016/j.bbrc.2005.08.066, PMID: 16129416

Yan G, Yan R, Chen C, Chen C, Zhao Y, Qin W, Veldman MB, Li S, Lin S. 2019. Engineering vascularized skeletal muscle tissue with transcriptional factor ETV2-induced autologous endothelial cells. *Protein & Cell* **10**:217–222. DOI: https://doi.org/10.1007/s13238-018-0542-7, PMID: 29687363

Young MD, Behjati S. 2020. SoupX removes ambient RNA contamination from droplet-based single-cell RNA sequencing data. *GigaScience* **9**:giaa151. DOI: https://doi.org/10.1093/gigascience/giaa151, PMID: 33367645

Yue L, Wan R, Luan S, Zeng W, Cheung TH. 2020. Dek modulates global intron retention during muscle stem cells quiescence exit. *Developmental Cell* **53**:661–676. DOI: https://doi.org/10.1016/j.devcel.2020.05.006, PMID: 32502396

Zhang MJ, Ntranos V, Tse D. 2020. Determining sequencing depth in a single-cell RNA-seq experiment. *Nature Communications* **11**:774. DOI: https://doi.org/10.1038/s41467-020-14482-y, PMID: 32034137

Zheng B, Cao B, Crisan M, Sun B, Li G, Logar A, Yap S, Pollett JB, Drowley L, Cassino T, Gharaibeh B, Deasy BM, Huard J, Péault B. 2007. Prospective identification of myogenic endothelial cells in human skeletal muscle. *Nature Biotechnology* **25**:1025–1034. DOI: https://doi.org/10.1038/nbt1334, PMID: 17767154

Appendix 1

Appendix 1—key resources table

Reagent type (species) or resource	Designation	Source or reference	Identifiers	Additional information
Strain (*Mus musculus*)	Flt1LoxP/LoxP	The Jackson Laboratory	JAX: 028098	Mouse line obtained from Guo-Hua Fong
Strain (*Mus musculus*)	VEGFA+/Hyper	The Jackson Laboratory	JAX: 027314	
Strain (*Mus musculus*)	Pax7CreERT2/+	The Jackson Laboratory	JAX: 017763	
Strain (*Mus musculus*)	mdx5cv	The Jackson Laboratory	JAX: 002379	
Strain (*Mus musculus*)	Flk1GFP	The Jackson Laboratory	JAX: 017006	Mouse line obtained from Masatsugu Ema
Strain (*Mus musculus*)	R26RtdT	The Jackson Laboratory	JAX: 007909	
Strain (*Mus musculus*)	VEGFALoxP/LoxP			Mouse line obtained from Napoleone Ferrara
Genetic reagent	Lentiviral pCCL-E4ORF1	PMID:20972423		Viral vector production
Genetic reagent	Lentiviral pCCL-myrAkt1	PMID:20972423		Viral vector production
Genetic reagent	pCMV-VSV-G	Addgene	8454	Viral vector production
Genetic reagent	pRSV-Rev	Addgene	12253	Viral vector production
Genetic reagent	pMDLg/pRRE	Addgene	12251	Viral vector production
Genetic reagent	RNAscope Probe - Mm-Flt1 (C1)	ACDBio	415541	RNAscope
Cell line (*Homo sapiens*)	293 FT	ThermoFisher Scoentific	R70007	Viral vector production
Cell line (*Mus musculus*)	C2C12	American Type Culture Collection (ATCC)	CRL-1772	MuSC line
Cell line (*Mus musculus*)	bEnd.3	American Type Culture Collection (ATCC)	CRL-2299	EC line
Cell line (*Mus musculus*)	C166	American Type Culture Collection (ATCC)	CRL-2581	EC line
Antibody	Anti-CD31-PE (Rat monoclonal)	ThermoFisher Scientific	12-0311-82; RRID: AB_465632	1:200
Antibody	Anti-CD45-PE (Rat monoclonal)	ThermoFisher Scientific	12-0451-81; RRID: AB_465668	1:200
Antibody	Anti-Sca-1-PE (Rat monoclonal)	ThermoFisher Scientific	A18486; RRID: AB_2535332	1:200
Antibody	Anti-FLT1 (Mouse monoclonal)	R&D systems	MAB4711; RRID: AB_2107038	1:200
Antibody	Anti-FLT1-APC (Rat monoclonal)	R&D systems	FAB4711A; RRID: AB_622149	1:200
Antibody	Anti-FLK1 (Rat monoclonal)	BD Biosceinces	555307; RRID: AB_395720	1:200
Antibody	Anti-FLK1-APC (Rat monoclonal)	BD Biosceinces	560070; RRID: C28AB_1645226	1:200
Antibody	Anti-VE-cadherin (Rat monoclonal)	BD Biosciences	555289; RRID: AB_2244723	1:200

Appendix 1 Continued on next page

Appendix 1 Continued

Reagent type (species) or resource	Designation	Source or reference	Identifiers	Additional information
Antibody	Anti-NRP1 (Rabbit monoclonal)	Cell Signaling Technology	3725; RRID:AB_2155231	1:200
Antibody	Anti-NRP1-APC (Rat monoclonal)	R&D systems	FAB5994A	1:200
Antibody	Anti-NRP2 (Rabbit monoclonal)	Cell Signaling Technology	3366; RRID: AB_2155250	1:200
Antibody	Anti-NRP2-APC (Mouse monoclonal)	R&D systems	FAB22151A; RRID: AB_10973479	1:200
Antibody	Anti-Sca-1-PE (Rat monoclonal)	eBiosciences	12-5981-81; RRID: AB_466085	1:200
Antibody	Anti-integrin a7-biotin (Mouse monoclonal)	Miltenyi Biotec	130-101-979; RRID: AB_2652472	1:200
Antibody	Anti-IgG-APC (Mouse)	ThermoFisher Scientific	PA5-33237; RRID: AB_2550652	1:200
Antibody	Anti-IgG-APC (Rat)	ThermoFisher Scientific	17-4321-81; RRID: AB_470181	1:200
Antibody	Anti-MyHC (Mouse monoclonal)	Developmental Study Hybridoma Bank	MF-20; RRID: AB_2147781	1:50
Antibody	Anti-MyoD (Mouse monoclonal)	DAKO	M3512; RRID: AB_2148874	1:200
Antibody	Anti-Pax7 (Mouse monoclonal)	Developmental Study Hybridoma Bank	PAX7; RRID: AB_528428	1:20
Antibody	Anti-pAKT (Rabbit monoclonal)	Cell Signaling	4060; RRID: AB_2315049	1:500
Antibody	Anti-VEGFA (Rabbit monoclonal)	Abcam	Ab52917; RRID: AB_883427	1:500
Antibody	Anti-mouse IgG Alexa488	ThermoFisher Scientific	A-11001; RRID: AB_2534069	1:1000
Antibody	Anti-rat IgG Alexa488	ThermoFisher Scientific	A-11006; RRID: AB_141373	1:1000
Antibody	Anti-rabbit IgG Alexa488	ThermoFisher Scientific	A-11008; RRID: AB_143165	1:1000
Antibody	Anti-rabbit IgG Alexa568	ThermoFisher Scientific	A-11011; RRID: AB_143157	1:1000
Antibody	Anti-mouse IgG Alexa568	ThermoFisher Scientific	A-11004; RRID: AB_2534072	1:1000
Antibody	Anti-rat IgG Alexa568	ThermoFisher Scientific	A-11077; RRID: AB_2534121	1:1000
Antibody	Anti-biotin beads	Miltenyi Biotec	130-090-485; RRID: AB_244365	MACS (1:500)
Antibody	Anti-PE beads	Miltenyi Biotec	130-048-801; RRID: AB_244373	MACS (1:500)
Antibody	Anti-Activated Caspase-3	Abcam	ab214430; RRID: AB_2938798	1:200
Antibody	Anti-phosphoAKT1	Cell Signaling	4060; RRID: AB_2315049	1:200 for IHC, 1:1000 for WB
Antibody	Anti-GAPDH HRP conjugated	Cell Signaling	3683; RRID: AB_1642205	1:10000

Appendix 1 Continued on next page

Appendix 1 Continued

Reagent type (species) or resource	Designation	Source or reference	Identifiers	Additional information
Antibody	Anti-eMHC (Mouse monoclonal)	Developmental Study Hybridoma Bank	F1.652; RRID: AB_528358	1:200
Antibody	Anti-Laminin-2 (Rat monoclonal)	MilliporeSigma	L0663; RRID: AB_477153	1:500
Sequence-based reagent (Oligo DNA)	TTAAACGAACGTACTTGCAGATG	Integrated DNA Technologies (IDT)	N/A	qPCR Vegfa 92 bp (Forward)
Sequence-based reagent (Oligo DNA)	AGAGGTCTGGTTCCCGAAA	Integrated DNA Technologies (IDT)	N/A	qPCR Vegfa 92 bp (Reverse)
Sequence-based reagent (Oligo DNA)	GCAGAGCCAGGAACATATACACA	Integrated DNA Technologies (IDT)	N/A	qPCR mFlt1 103 bp(Forward)
Sequence-based reagent (Oligo DNA)	GAGATCCGAGAGAAAATGGC CTTT	Integrated DNA Technologies (IDT)	N/A	qPCR mFlt1 103 bp (Reverse)
Sequence-based reagent (Oligo DNA)	GCAGAGCCAGGAACATATACACA	Integrated DNA Technologies (IDT)	N/A	qPCR sFlt1 73 bp (Forward)
Sequence-based reagent (Oligo DNA)	CAGTGCTCACCTCTAACG	Integrated DNA Technologies (IDT)	N/A	qPCR sFlt1 73 bp (Reverse)
Sequence-based reagent (Oligo DNA)	CAGTGGTACTGGCAGCTAGAAG	Integrated DNA Technologies (IDT)	N/A	qPCR KDR/Flk1 66 bp (Forward)
Sequence-based reagent (Oligo DNA)	ACAAGCATACGGGCTTGTTT	Integrated DNA Technologies (IDT)	N/A	qPCR KDR/Flk1 66 bp (Reverse)
Sequence-based reagent (Oligo DNA)	TCCTGGGAAACTGGTATATC TATGA	Integrated DNA Technologies (IDT)	N/A	qPCR Nrp1 75 bp (Forward)
Sequence-based reagent (Oligo DNA)	CATTCCAGAGCAAGGATAATCTG	Integrated DNA Technologies (IDT)	N/A	qPCR Nrp1 75 bp (Reverse)
Sequence-based reagent (Oligo DNA)	ATGGCTGGACACCCAATTT	Integrated DNA Technologies (IDT)	N/A	qPCR Nrp2 67 bp (Forward)
Sequence-based reagent (Oligo DNA)	ATGGTTAGGAAGCGCAGGT	Integrated DNA Technologies (IDT)	N/A	qPCR Nrp2 67 bp (Reverse)
Sequence-based reagent (Oligo DNA)	CACCTGGAGAGGATGAAGAA GAA	Integrated DNA Technologies (IDT)	N/A	qPCR Myh3 298 bp (Forward)
Sequence-based reagent (Oligo DNA)	AAGACTTGACTTTCACTTGGAGTT TA TC	Integrated DNA Technologies (IDT)	N/A	qPCR Myh3 298 bp (Reverse)
Sequence-based reagent (Oligo DNA)	TTCGGAAGCTCCTTCTGTTT	Integrated DNA Technologies (IDT)	N/A	qPCR Htatsf1 79 bp (Forward)
Sequence-based reagent (Oligo DNA)	CCAGAGTCTGAATACAATGGTCA	Integrated DNA Technologies (IDT)	N/A	qPCR Htatsf1 79 bp (Reverse)
Sequence-based reagent (Oligo DNA)	CGCACGGCCGGTACAGTGAA ACTG	Integrated DNA Technologies (IDT)	N/A	qPCR 18 S rRNA 343 bp (Forward)

Appendix 1 Continued on next page

Appendix 1 Continued

Reagent type (species) or resource	Designation	Source or reference	Identifiers	Additional information
Sequence-based reagent (Oligo DNA)	CGCACGGCCGGTACAGTGAA ACTG	Integrated DNA Technologies (IDT)	N/A	qPCR 18 S rRNA 343 bp (Reverse)
Sequence-based reagent (Oligo DNA)	CTTGCTCACCATGGTCAGCT GCTG	Integrated DNA Technologies (IDT)	N/A	Genotyping Myh3 Exon1 WT/ MUT-103bp (Reverse)
Sequence-based reagent (Oligo DNA)	CACTTTTAACTTCGACCCTGAGCC	Integrated DNA Technologies (IDT)	N/A	Genotyping Myh3 Exon2 WT/ MUT-103bp (Reverse)
Sequence-based reagent (Oligo DNA)	GGCCAGACTCTCTTTCTCAA GTGC	Integrated DNA Technologies (IDT)	N/A	Genotyping Myh3 Exon2 WT-135bp (Forward)
Sequence-based reagent (Oligo DNA)	GCAGAATTGCCTGTTATCCCTCCC	Integrated DNA Technologies (IDT)	N/A	Genotyping Myh3 Exon3 WT-135bp (Reverse)
Sequence-based reagent (Oligo DNA)	GCTGCTGTTGATTACCTGGC	Integrated DNA Technologies (IDT)	N/A	Genotyping Pax7CreERT2 (Common)
Sequence-based reagent (Oligo DNA)	CAAAAGACGGCAATATGGTG	Integrated DNA Technologies (IDT)	N/A	Genotying Pax7CreERT2 MUT-235bp (Reverse)
Sequence-based reagent (Oligo DNA)	CTGCACTGAGACAGGACCG	Integrated DNA Technologies (IDT)	N/A	Genotying Pax7CreERT2 WT-419bp (Reverse)
Sequence-based reagent (Oligo DNA)	GGCATTAAAGCAGCGTATCC	Integrated DNA Technologies (IDT)	N/A	Genotying R26RtdT (9103) MUT-196bp (Forward)
Sequence-based reagent (Oligo DNA)	CTGTTCCTGTACGGCATGG	Integrated DNA Technologies (IDT)	N/A	Genotying R26RtdT (9105) MUT-196bp (Reverse)
Sequence-based reagent (Oligo DNA)	AAGGGAGCTGCAGTGGAGTA	Integrated DNA Technologies (IDT)	N/A	Genotying R26RtdT (9020) WT-297bp (Forward)
Sequence-based reagent (Oligo DNA)	CCGAAAATCTGTGGGAAGTC	Integrated DNA Technologies (IDT)	N/A	Genotying R26RtdT (9021) WT-297bp (Reserve)
Sequence-based reagent (Oligo DNA)	AGCAGCACGACTTCTTCAAG TCCG	Integrated DNA Technologies (IDT)	N/A	Genotying Flk1GFP-161bp (Forward)
Sequence-based reagent (Oligo DNA)	CTCCTTGAAGTCGATGCCCT TCAG	Integrated DNA Technologies (IDT)	N/A	Genotying Flk1GFP-161bp (Reserve)
Sequence-based reagent (Oligo DNA)	CGCTTTTTGTCAGTCATCTTCA	Integrated DNA Technologies (IDT)	N/A	Genotying Flt1Loxp/Loxp (FlpeEX3F) WT-223bp/MUT-641bp (Forward)
Sequence-based reagent (Oligo DNA)	GTGCCACTGACCTAACATGT AAGAG	Integrated DNA Technologies (IDT)	N/A	Genotying Flt1Loxp/Loxp (FlpeInt3R) WT-223bp/MUT-641bp (Reverse)
Sequence-based reagent (Oligo DNA)	CCA TAG ATG TGA CAA GCC AAG	Integrated DNA Technologies (IDT)	N/A	Genotyping VEGFAHyper (24286) WT-254bp (Forward)
Sequence-based reagent (Oligo DNA)	ACC CGG GGA TCC TCT AGA AC	Integrated DNA Technologies (IDT)	N/A	Genotyping VEGFAHyper (25307) MUT-199bp (Forward)

Appendix 1 Continued on next page

Appendix 1 Continued

Reagent type (species) or resource	Designation	Source or reference	Identifiers	Additional information
Sequence-based reagent (Oligo DNA)	GAC CGT GCT TGG TCA CCT	Integrated DNA Technologies (IDT)	N/A	Genotyping VEGFAHyper (25308, Common) WT-254bp/ MUT-199bp (Reverse)
Sequence-based reagent (Oligo DNA)	CCTGGCCCTCAAGTACACCTT	Integrated DNA Technologies (IDT)	N/A	VEGFALoxP/LoxP (muVEGF 419 .F) WT-106bp/MUT-148bp (Forward)
Sequence-based reagent (Oligo DNA)	TCCGTACGACGCATTTCTAG	Integrated DNA Technologies (IDT)	N/A	VEGFALoxP/LoxP (muVEGF 567 .R) WT-106bp/MUT-148bp (Reverse)
Sequence-based reagent (Oligo DNA)	GAAGCTCCCAGAGACAAGTC	Integrated DNA Technologies (IDT)	N/A	mdx5cv (0981) WT/MUT-180bp (Forward)
Sequence-based reagent (Oligo DNA)	TCATGAGCATGAAACTGTTCTT	Integrated DNA Technologies (IDT)	N/A	mdx5cv (0981) WT/MUT-180bp (Reverse)
Commercial assay or kit	GoTaq qPCR Master Mix	Promega,	A6002	qPCR
Commercial assay or kit	Click-iT EdU Alexa Fluor 488 Imaging Kit	Thermo Scientific	C10337	EdU staining
Commercial assay or kit	Crystal violet Assay Kit	Abcam	ab232855	Cell viability assay
Commercial assay or kit	Transcriptor First Strand cDNA Synthesis Kit	Roche-Sigma-Aldrich	4379012001	cDNA synthesis
Commercial assay or kit	Annexin V-Biotin Apoptosis Detection Kit	eBioscience	BMS500BT-100	Appotosis assay
Commercial assay or kit	DirectZolTM RNA Microprep Kit	Zymo Research	R2062	RNA isolation
Commercial assay or kit	Midi Fast Ion Plasmid Kit	IBI Scientific	IB47111	Plasmid DNA isolation
Commercial assay or kit	H&E Staining Kit	Abcam	ab245880	Histology
Commercial assay or kit	SuperSignal West Femto chemiluminescent substrate	Fisher Scientific	PI37074	Western Blotting
Commercial assay or kit	NE-PER Nuclear and Cytoplasmic Extraction reagents	Thermo Fisher Scientific	78833	Protein extraction
Chemical compound, drug	bFGF	Thermo Fisher Scientific	PHG0263	MuSC culture (20 ng/ml)
Chemical compound, drug	Bovine serum albumin (BSA)	Jackson Immuno Research	10001620	FACS/Immunostaining (1–2%)
Chemical compound, drug	Chicken embryo extract	MP-Biomedical	92850145	Single muscle fiber culture (0.5%)
Chemical compound, drug	Collagen	BD Biosciences	354236	Culture dish coating (0.01%)
Chemical compound, drug	Collagenase type I	Sigma-Aldrich	C0130	Single myofiber isolation (0.2%)
Chemical compound, drug	Collagenase type II	Worthington Biochemical Corp	CLD-2	FACS and MuSC/ES isolation (0.2%)
Chemical compound, drug	DAPI (4',6-diamidino-2-phenylindole dihydrochloride)	Thermo Fisher Scientific	D1306	DNA staining (1 µg/ml)
Chemical compound, drug	Dulbecco's Modified Eagle's Medium (DMEM)	Thermo Fisher Scientific	41966	Single myofiber and ES culture

Appendix 1 Continued on next page

Appendix 1 Continued

Reagent type (species) or resource	Designation	Source or reference	Identifiers	Additional information
Chemical compound, drug	EdU	Thermo Fisher Scientific	C10340	Cell proliferation (1 µM)
Chemical compound, drug	F-10 Ham's media	Sigma-Aldrich	N6635	MuSC culture
Chemical compound, drug	Fetal calf serum (FCS)	Atlas Biological	FS-0500-AD	MuSC/EC/Single muscle fiber culture (10% or 20%)
Chemical compound, drug	Horse serum	Thermo Fisher Scientific	26050088	2% (coating), 5% (Differentiation culture)
Chemical compound, drug	L-glutamine	Thermo Fisher Scientific	25030	Culture medium (20 mM)
Chemical compound, drug	Matrigel	Corning Life Sciences	354230	Single muscle fiber culture (1:20)
Chemical compound, drug	Penicillin/streptomycin	Life Technologies	15140	Culture medium (1 X)
Chemical compound, drug	Tamoxifen (TMX)	Sigma-Aldrich	T5648	Cre recombinase (60 mg/kg i.p.)
Chemical compound, drug	4-hydroxy tamoxifen (4-OHT)	Sigma-Aldrich	H6278	Culture (1 µM)
Chemical compound, drug	Cardiotoxin (CTX)	Sigma-Aldrich	V9125	Muscle injury (10 µM)
Chemical compound, drug	DraIII	New England Biolabs	R3510S	DNA digestion (500 U/ml)
Chemical compound, drug	ZombieNIR	Biolegends	423105	FACS (0.1%)
Chemical compound, drug	recombinant VEGFA	R&D Systems	493 MV	Culture (2–100 ng/ml)
Chemical compound, drug	Thapsigargin	Sigma-Aldrich	T9033	Culture (1 µM)
Chemical compound, drug	FLT1-FC	R&D Systems	7756-FL	Culture (100 ng/ml)
Chemical compound, drug	ZM306416	R&D Systems	2499/1	Culture (3 µM)
Chemical compound, drug	SU5402	R&D Systems	3300/1	Culture (10 µM)
Chemical compound, drug	EG00229	R&D Systems	6986/10	Culture (30 µM)
Chemical compound, drug	PolyJet transfection reagent	Signagen Laboratories	SL100688	DNA transfection (10 µl for 6 cm plate)
Chemical compound, drug	Polybrene	MilliporeSigma	H9268	Viral infection (0.8 µg/ml)
Chemical compound, drug	Saponin	ThermoFisher Scientific	ICN10285525	Immunostaining (0.01%)
Chemical compound, drug	Direct Red 80	Sigma-Aldrich	365548	Histology (0.1%)
Chemical compound, drug	Proteinase K	Sigma-Aldrich	P2308	DNA isolation (40 µg/mL)
Chemical compound, drug	Oil Red O solution	Sigma-Aldrich	O1391-250ML	Histology (0.5%)
Chemical compound, drug	Trizol	ThermoFisher Scientific	15596026	RNA isolation

Appendix 1 Continued on next page

Appendix 1 Continued

Reagent type (species) or resource	Designation	Source or reference	Identifiers	Additional information
Software, algorithm	Photoshop 2020	Adobe	https://www.adobe.com/products/photoshop.html	Imaging analysis
Software, algorithm	Fiji	NIH	https://imagej.net/software/fiji/	Imaging analysis
Software, algorithm	cellSens Entry 1.11	Olympus	https://www.olympus-lifescience.com/en/software/cellsens/	Microscopy
Software, algorithm	Prism 9	GraphPad	https://www.graphpad.com/support/faq/prism-900-release-notes/	Data analysis and statistics
Software, algorithm	RStudio	RStudio	https://www.rstudio.com	Data analysis and statistics
Software, algorithm	Autodesk Graphic	Autodesk	https://www.graphic.com	Vector design
Software, algorithm	BioRender: Scientific Image and Illustration Software	BioRender.com	https://www.biorender.com	Illustrator
Other	Anti-biotin beads	Miltenyi Biotec	130-090-485; RRID:AB_244365	MACS
Other	Anti-PE beads	Miltenyi Biotec	130-048-801; RRID:AB_244373	MACS
Other	Cell culture plate, 24 well	Sarstedt	83.3922	Single myofiber culture
Other	Tissue culture dish	Sarstedt	83.39	MuSC/ES culture
Other	Tissue culture dish	Sarstedt	83.3901	MuSC/ES culture
Other	Tissue culture dish	Sarstedt	83.3902	MuSC/ES culture
Other	LD column	Miltenyi Biotec	130-042-901	MACS
Other	MS column	Miltenyi Biotec	130-042-201	MACS
Other	Fortessa X-20	BD Biosciences		FACS
Other	BD FACSAria	BD Biosciences		FACS
Other	moorLabTM laser Doppler	Moor Instruments	MOORVMS-LDF	Laser Doppler flow
Other	Grip strength meter	Columbus Instruments	1027CSM-D54	Forelimb muscle force
Other	iBright FL1500	ThermoFisher Scientific	A44115	Western blotting
Other	Olympus IX81 Inverted Fluorescense microscope	Olympus		Microscope
Other	Olympus BX51 Fluorescense microscope	Olympus		Microscope